

RESULTS OF SCATTEROMETER SYSTEMS ANALYSIS  
FOR NASA/MSC EARTH OBSERVATION  
SENSOR EVALUATION PROGRAM

by

K. Krishen, N. Vlahos, O. Brandt  
Earth Observation Division  
Lockheed Electronics Company

and

G. Graybeal  
NASA/MSC Earth Observation Division

November 1970

ABSTRACT

Radar scatterometers have applications in the NASA/MSC Earth Observation Aircraft Program. Over a period of several years, several missions have been flown over both land and ocean. In this paper a systems evaluation of the NASA/MSC 13.3 GHz Scatterometer System is presented. The effects of phase error between the scatterometer channels, antenna pattern deviations, aircraft attitude deviations, environmental changes, and other related factors such as processing errors, system repeatability, and propeller modulation, were established. Furthermore, the reduction in system errors and calibration improvement was investigated by taking into account these parameter deviations. Typical scatterometer data samples are presented.

ACKNOWLEDGMENTS

The work reported in this paper was supported by NASA/MSC under contract NAS 9-5191. The hardware test data were provided by the Telecommunications Systems Division of NASA/MSC. The cooperation of J. Fisher and J. Skipworth (Computation and Analysis Division) in processing and analysis of test tape data is appreciated.

## INTRODUCTION

The airborne 13.3-GHz Single Polarized Scatterometer is currently used by the NASA/MSC Earth Observation Division to investigate its use for the following applications:

- Study of wind fields and resulting sea waves; the dependence of radar scattering cross section ( $\sigma_0$ ) on parameters such as local wind velocity, significant wave height, and sea spectrum
- Discrimination of arctic ice types
- Study characteristics of the earth's surface in order to determine and catalog reflectivity data for various types of land areas for geoscience investigations.

These studies are aimed at correlating surface composition and shape with backscattering cross sections as a function of incident angle, polarization, and frequency.

The 13.3-GHz scatterometer is a continuous-wave doppler radar system, designed to measure reflectivity per unit area as a function of the angle of incidence ( $\theta$ ). The scatterometer antenna illuminates a fan-shaped area (approximately  $120^\circ$  along the aircraft flightpath), and the data is gathered for vertical-transmit, vertical-receive polarization states only. As a result of the forward motion of the aircraft, doppler frequency shifts are introduced and the signal returned by a ground resolution cell can be retrieved by bandpass filtering at the corresponding doppler frequencies.

Several scatterometer missions have been flown by NASA/MSC over several years. In the process of data interpretation and correlation from various missions and scatterometers, several problem areas were evident. These problems were related to the scatterometer hardware parameter evaluation, the data processing, and the antenna pattern parametric evaluation. Consequently, a systems evaluation was undertaken within the Earth Observation Division at MSC for the 13.3-GHz Single Polarized System. In this paper a review of the results of this evaluation is presented.

SENSOR TEST EVALUATION

A circuit diagram of the 13.3-GHz system is shown in Figure 1. A functional and equipment description of the system is contained in reference 1. To define the terminology used in this paper, a brief description of the system follows.

The radar-frequency energy is radiated by an antenna which has a wide fore-and-aft beam and a narrow transverse beam (Figure 2). The returned energy may be separated using the doppler equation as a function of incidence angle

$$f_d = \frac{2V}{\lambda} \sin \theta \quad (1)$$

where

V = aircraft ground velocity

$\lambda$  = wavelength of the transmitted power

$\theta$  = angle of incidence.

The returned energy is received from all angles of incidence simultaneously and is divided equally into two channels, one of which is 90° out of phase with the other. The data for each channel, detected by a direct-to-audio technique, are amplified and recorded on an FM tape recorder. The fore-and-aft beam data are separated by use of a sign sensing technique (reference 2). To calibrate the system a ferrite modulator is used to provide an absolute power reference level of the transmitted signal. The  $\sigma_0$  versus  $\theta$  information is obtained by subtracting known system losses and aircraft attitude and velocity factors and comparing the remainder with a reference signal level.

The radar cross section per unit area is given by the equation

$$\sigma_0(\theta) = \frac{P_R}{P_T} \frac{2(4\pi)^3}{\lambda^3} \cdot \frac{Vh^2}{\Delta f_d} \cdot \frac{1}{\int_{-\psi_1}^{\psi_2} G_T(\psi)_\theta G_R(\psi)_\theta d\psi} \quad (2)$$

where

$P_T$  = transmitted power

$P_R$  = power received in the doppler window defined by  $\Delta f_d$

$G_T, G_R$  = transmitting antenna and receiving antenna gain, respectively, as a function of  $\theta$  (incident angle), and  $\psi$  (cross track angle)

$h$  = altitude of the aircraft.

Equation (2) may be rearranged for computer calculations as

$$\sigma_0(\theta) = RC + 20 \log h + 10 \log V + 20 \log \frac{E_i}{E_r} + 10 \log \frac{BW_R}{BW_i} + R(D) - G_0^2 F'(\theta) + Z(\theta) \quad (3)$$

where

$RC$  = radar offset constant

$h$  = aircraft height

$E_i$  = average radar data at  $i$ th filter

$E_r$  = average reference data

$BW_i$  = bandwidth of  $i$ th filter

$R(D)$  = system rolloff

$Z(\theta)$  = any system errors  $f(\theta)$  which can be determined

$G_0^2 F'(\theta)$  = two-way antenna gain

$BW_R$  = reference bandwidth

The radar offset constant (RC) is computed from the following equation

$$RC = 10 \log_{10} 2(4\pi)^3 + FMC - 10 \log_{10} P_T - 30 \log_{10} \lambda \quad (4)$$

where

FMC = ferrite modulator constant.

As a result of the time element involved in the data gathering program, several factors can contribute to a change in the scatterometer system. As a consequence an investigation of mission-to-mission consistency and repeatability of the scatterometer data was undertaken. In this section a summary of the hardware test results in connection with the consistency and repeatability study is presented.

#### KLYSTRON POWER

In the process of checking the klystron power output for missions 70 and 88, it was found that the quoted output klystron power for these two missions was 1.6 watts and 2.1 watts, respectively. However, in the program for computing the scattering cross section, a power of 1.5 watts was assumed for both missions. To reflect correct transmitted power the previously processed data for mission 88 was adjusted by 1.5 dB. For the succeeding missions two new klystrons were obtained by NASA/MSC (S/Ns 235 and 251). Environmental testing also was conducted on both klystrons where the ambient air temperature was taken between 0° F to 100° F with the klystron body temperature varying from 30° F to 130° F. Figure 3 shows results wherein the output power is reasonably constant for these klystrons at 31.3 dBm (S/N 235) and 31.6 dBm (S/N 251). The long term frequency shift is approximately 26 MHz.

#### FERRITE MODULATOR

The ferrite modulator was tested for temperature stability. The ferrite modulator, measured over a temperature range of 0° F to 200° F, was found constant. The recently measured value of the ferrite modulator constant is -125.72 dB, while the value measured 2 years ago was -127.7 dB. The proper ferrite modulator constant was reflected in the radar offset constant for mission 119 and subsequent missions.

## WAVEGUIDE INSERTION LOSSES

The 13.3-GHz system was tested for insertion losses in the waveguide plumbing. These losses, shown in Table I, determine the power levels. Adjustments in the radar offset constant, reflecting the latest loss measurements, indicate good consistency of the values of these losses.

TABLE I.- WAVEGUIDE INSERTION LOSSES

13.3-GHz Single Polarized Scatterometer Waveguide Insertion Loss Test Data (reference Figure 1):

Receiver antenna (1) to diode mixer (5): 3.3 dB  
 Receiver antenna (1) to diode mixer (6): 3.6 dB  
 Klystron (2) to transmit antenna port (3): 0.5 dB  
 Klystron (2) to diode mixer port (6): 37.4 dB  
 Klystron (2) to diode mixer port (5): 36.5 dB

## ANTENNA BORESIGHT

To process data from missions 88 and 70, the 13.3-GHz scatterometer antenna was originally boresighted down (fore beam down) by  $3^\circ$  from the NP3A aircraft centerline. In reviewing the recent boresight data it was noted that the antenna was boresighted down by only  $1.5^\circ$  (fore beam down). The computer program therefore was modified to reflect the  $1.5^\circ$  boresight alignment.

## PROPELLER MODULATION

Propeller modulation was noticed at 20,000-foot altitude on the NP3A aircraft. The frequency spectrum of the propeller modulation corresponds to about  $42^\circ$  to  $60^\circ$  angle of incidence for an aircraft speed of 200 knots. With the present klystron, the effect of propeller modulation is not serious at altitudes below 5,000 feet for high sea states. Further editing of the effect of propeller modulation can be achieved by properly selecting the doppler frequencies in this interference band.

## ROLLOFF CONSTANT CURVES

The 13.3-GHz Single Polarized Scatterometer System's amplifier's four attenuators were checked for frequency response. This resulted in new rolloff curves for use in the computer processing program. Figure 4 shows a comparison of previous and newly measured values. The new rolloff constants have to be taken for all missions succeeding mission 88.

## ANTENNA PATTERN MEASUREMENTS

The 13.3-GHz Single Polarized Scatterometer System was designed and fabricated in early 1965 and adopted by the NASA Apollo Program to determine lunar reflectivity characteristics by overflying selected test sites. The system was a breadboard design with emphasis placed upon relative rather than absolute measurements. The antenna measurements were made on a two-way basis using a CV-240 aircraft mockup. At the termination of the lunar reflectivity program, this sensor was installed on board the NP3A and the CV-240 aircraft for Earth Resources studies. The data for all sea state missions after mission 60 were collected aboard the NP3A aircraft.

In reviewing the data from missions 70 and 88 (with CV-240 mockup patterns), some anomalies were observed in the power spectral density plots (return versus doppler shift). It was recommended that patterns with the NP3A mockup be utilized in the data reduction program. Further study of the data from missions 70 and 88 indicated that in order to reduce errors in scattering cross section, additional antenna pattern data would be required. The CV-240 mockup measurements were made for a long track of  $\pm 70^\circ$  at  $1^\circ$  intervals on the principal axis only, and the cross track data was taken every  $10^\circ$  along the principal axis (reference 1). New antenna patterns with the NP3A mockup were obtained on a better range (0.1 dB accuracy in measurement). These patterns, obtained in September 1969, were made for  $\pm 70^\circ$ , every  $0.2^\circ$  on the long track and in the cross track ( $\psi$ ,  $\pm 10^\circ$ ) in increments of  $0.5^\circ$  out to  $\pm 3^\circ$  and  $1^\circ$  increments from  $\pm 3^\circ$  to  $\pm 10^\circ$ .

Figure 5 illustrates the differences in antenna patterns. The value of  $G_{0F}^2(\theta)$  is calculated with 3 dB beamwidth points (reference 1). "Old  $G_{0F}^2(\theta)$ " refers to the CV-240 mockup pattern given in reference 1; "Redop 1" refers to patterns obtained with the NP3A mockup with no change in radome configuration; and "Redop 1 modified" (used in all missions after mission 88) refers to patterns with the NP3A mockup after the antenna was cleaned and a new radome was fabricated.

Differences up to 5 dB are indicated in the antenna gain values. The study of antenna pattern integration into the processing program (in the next section) shows that the elaborate new antenna gain measurements have made it possible to reduce the errors in scattering cross section resulting from insufficient antenna gain values.

#### TAPE RECORDER ADJUSTMENTS

A test was conducted on the Ampex FR-1900 Tape Recorder in the Data Techniques Laboratory, recording on tracks 2 and 4. The results showed an azimuth adjustment of  $\pm 14$  microseconds at 30-ips tape speed. This means that the azimuth adjustment on this tape recorder can shift the phase relationship between channel 1 and channel 2 by about  $\pm 50^\circ$  at 10 kHz. An analysis of phase error between channels 1 and 2 (see next section) shows that this phase shift contributes a significant error to the scattering cross-section values. The results of the FR-1900 study made it clear that a means of adjusting the Computation and Analysis Division (CAD) playback tape recorders azimuth verniers to a zero phase reference was necessary.

Measurements on the 13.3-GHz system showed that the land and sea filters were matched and that the only significant skew or phase error was caused by the tape recorder record head alignment. A test tape was made on board the NP3A aircraft. A sweep oscillator output was fed into the 13.3-GHz system at the preamplifier output location (Figure 1). The signal (a 12-kHz sine wave and a sine sweep from 500 Hz to 12 kHz) passed through the sea/land filters and postamplifiers, and was recorded on the Ampex AR-1600 tape recorder.

This tape was analyzed in the Data Techniques Laboratory. The results showed that the phase error increased linearly with frequency and that it could be nulled with the reproduce tape recorder azimuth adjust. Based on this study, a method of adjusting the CAD tape recorders for a zero phase error was outlined. The method consists of recording an in-phase 10-kHz sine wave on the two channels and while monitoring these channels with a dual beam oscilloscope at the playback station, adjusting the azimuth control of the playback recorder for an in-phase condition (reference 3). This adjustment assures that no phase shift is introduced into the audio and recording portion of the 13.3-GHz Scatterometer System.

## SYSTEMS PERFORMANCE EVALUATION

During the evaluation of the systems performance, three areas appeared for further study. The first area was related to the inconsistencies in the previously reported circuit configurations. This is particularly important in separating the fore and aft beam data. The results of a study leading to the correct circuit configuration of the 13.3-GHz system is described. The second area was related to the effects of a phase shift error in the RF portion of the system. The third area of study was to investigate various methods for integrating the antenna pattern in the calculation of the scattering cross section.

### CIRCUIT CONFIGURATION FOR SIGN SENSING

Inconsistencies in the documentation of 13.3-GHz Single Polarized Scatterometer System configuration presented a task in determining fore and aft beam data. In particular, the following uncertainties were encountered:

- Which channel has the calibration signal?
- Which channel is phase-shifted by 90°?
- Is the phase shift leading or lagging?

One of the procedures developed to ascertain the correct fore and aft beam separation was the simulated doppler test. A positive or a negative doppler signal of 1 kHz was produced (Figure 6) by controlling the direction of rotation and speed of the motor. The doppler signals developed were at 13.3 GHz ( $\pm 1$  kHz) and of constant amplitude. The (+) sign corresponds to the fore-beam data and the (-) sign to the aft-beam data.

The data sequence consisted of 2 minutes of a positive 1-kHz doppler signal, followed by a period when the drive power was turned off, causing the positive 1-kHz signal to decrease in frequency to 0 Hz. Further, the preceding sequence was repeated with the motor drive reversed, thereby simulating negative 1 kHz, followed by a decreasing frequency signal to 0 Hz. The data were recorded on a magnetic tape. The data were processed using an analog processing procedure to check the power spectral density of the recorded signal.

The tape was processed utilizing the CAD digital computer program (reference 2). Figure 7 shows positive 1-kHz signal in the fore beam,

and Figure 8 shows the negative 1-kHz signal in the aft beam. It was concluded that the program was producing the correct doppler data. The fore beam data resulted from positive doppler and the aft beam from negative doppler, as the case should be. Furthermore, the calibration was on channel 1. At this time a problem arose as to the correct phase shift between channels 1 and 2. Further investigation into hardware plumbing using X-rays was conducted. The following conclusions were made:

- The phase shift was not introduced through the local oscillator
- The phase shift was introduced in the 3 dB coupler (Figure 9)
- The signal in channel 1 lags the channel 2 signal by 90°.

These conclusions are reflected in Figures 1 and 9.

#### PHASE SHIFT ERRORS

In validating the NASA/MSR 13.3-GHz Single Polarized Scatterometer data, it is essential that the influence of the system on the data be completely formulated. The phase shift between channels 1 and 2 is an important parameter of this system. The fore and aft beam data can be separated accurately if the amplitudes of the signals are equal for channels 1 and 2 before data processing and the phase difference between the two is 90°. However, there are several possible reasons why this phase difference can vary from 90°. The possible sources of error are (Figure 9):

1. Hybrid coupler output may not have 90° phase shift
2. Ferrite modulator error could be caused by temperature changes
3. Possible local oscillator phase difference at the input to the channels
4. Mixers and amplifiers could give unequal phase shift in the two channels
5. Tape recorders phase shift could be introduced through nonalignment.

The phase shift errors resulting from amplifiers, filters, and tape recorders have been checked and present no problem (see previous section). In the following paragraphs the errors in scattering cross section due to any phase shift errors in the RF portion of the system will be derived. The calculated values have been compared with measured values.

#### Mathematical Analysis of the RF Phase Shift

The received signals from fore and aft beam scattering at a particular angle of incidence are assumed to be, respectively

$$\begin{aligned} \sqrt{2} A_+(\omega_d, t) \cos [(\omega_T + \omega_d)t + \alpha(\omega_d, t)] \\ \sqrt{2} A_-(\omega_d, t) \cos [(\omega_T - \omega_d)t + \beta(\omega_d, t)] \end{aligned} \quad (5)$$

where

$\omega_T$  = the transmitter frequency

$\pm\omega_d$  = the doppler shift corresponding to fore and aft beam at a particular angle of incidence

$\alpha(\omega_d, t)$  = the transit phase shift introduced by the rough surface in the fore beam

$\beta(\omega_d, t)$  = the transit phase shift introduced by the rough surface in the aft beam

The output in channels 1 and 2 (Figure 9) is

$$\begin{aligned} \text{channel 1 (F}_1\text{)} &= k[A_+ \sin (\omega_d t + \alpha) + A_- \sin (-\omega_d t + \beta)] \\ \text{channel 2 (F}_2\text{)} &= k[A_+ \cos (\omega_d t + \alpha) + A_- \cos (-\omega_d t + \beta)] \end{aligned} \quad (6)$$

where

$k = 1/2[\text{channel transfer function/gain}]$ .

The value of  $A_+$  and  $A_-$  can be obtained by taking Fast Fourier Transform (FFT) of equation (6). After a few manipulations the values of  $A_+$  and  $A_-$  are given by

$$\begin{aligned} A_+^2 &= k^2 [\{\text{Re } f_1 - \text{Im } f_2\}^2 + \{\text{Re } f_2 + \text{Im } f_1\}^2] \\ A_-^2 &= k^2 [\{\text{Re } f_1 + \text{Im } f_2\}^2 + \{\text{Re } f_2 - \text{Im } f_1\}^2] \end{aligned} \quad (7)$$

where

$\text{Re } f_1$  is the real part of the FFT of channel 1

$\text{Im } f_2$  is the imaginary part of the FFT of channel 2, etc.

Now, the total RF phase shift between the two channels is assumed to be

$$(90 + \theta_m + \theta_e)$$

where  $\theta_m$  is the phase difference due to ferrite modulator, and  $\theta_e$  the total error due to other sources. The signal in channel 1 is mixed with  $\cos(\omega_T t + \theta_m)$  while the channel 2 signal is mixed with  $\cos(\omega_T t)$ . The resultant output at the end of channels 1 and 2 is, respectively

$$F_{1e} = k[A_+ \sin(\omega_d t + \theta_e + \alpha) + A_- \sin(-\omega_d t + \theta_e + \beta)] \quad (8)$$

$$F_{2e} = k[A_+ \cos(\omega_d t + \alpha) + A_- \cos(-\omega_d t + \beta)]$$

The FFT of equation (8), ignoring the negative frequency terms, yields

$$f_{1e} = \frac{k}{2} \left[ \left\{ A_+ \sin(\theta_e + \alpha) + A_- \sin(\theta_e + \beta) \right\} + j \left\{ A_+ \cos(\theta_e + \alpha) - A_- \cos(\theta_e + \beta) \right\} \right] \delta(\omega_d) \quad (9)$$

$$f_{2e} = \frac{k}{2} \left[ \left\{ A_+ \cos \alpha + A_- \cos \beta \right\} + j \left\{ A_- \sin \beta - A_+ \sin \alpha \right\} \right] \delta(\omega_d)$$

As a result of phase error, the values of fore and aft beam data are different from  $A_+$  and  $A_-$ . Consequently, the value of fore and aft beam signal is assumed to be, respectively

$$\begin{aligned} \sqrt{2} X_+(\omega_d, t) \cos [(\omega_T + \omega_d)t + m(\omega_d, t)] \\ \sqrt{2} X_-(\omega_d, t) \cos [(\omega_T - \omega_d)t + n(\omega_d, t)] \end{aligned} \quad (10)$$

The following equation can be obtained from equations (9) and (10)

$$\begin{aligned} X_+ \cos m &= \frac{k}{2} [A_+ \cos \alpha + A_- \cos \beta + A_+ \cos (\theta_e + \alpha) \\ &\quad - A_- \cos (\theta_e + \beta)] \\ X_+ \sin m &= \frac{k}{2} [A_+ \sin (\theta_e + \alpha) + A_- \sin (\theta_e + \beta) - A_- \sin \beta \\ &\quad + A_+ \sin \alpha] \\ X_- \cos m &= \frac{k}{2} [A_+ \cos \alpha + A_- \cos \beta - A_+ \cos (\theta_e + \alpha) \\ &\quad + A_- \cos (\theta_e + \beta)] \\ X_- \sin m &= \frac{k}{2} [A_+ \sin (\theta_e + \alpha) + A_- \sin (\theta_e + \beta) + A_- \sin \beta \\ &\quad - A_+ \sin \alpha] \end{aligned} \quad (11)$$

The following values can be obtained from equation (11)

$$\frac{X_+}{A_+} = \left[ \frac{1}{2} + \frac{P^2}{2} + \frac{P}{2} \cos (\alpha + \beta) + \left( \frac{1}{2} - \frac{P^2}{2} \right) \cos \theta_e - \frac{P}{2} \cos (\alpha + \beta + 2\theta_e) \right]^{1/2} \quad (12)$$

$$\frac{X_-}{A_-} = \left[ \frac{1}{2} + \frac{1}{2P^2} + \frac{1}{2P} \cos (\alpha + \beta) + \left( \frac{1}{2} - \frac{1}{2P^2} \right) \cos \theta_e - \frac{1}{2P} \cos (\alpha + \beta + 2\theta_e) \right]^{1/2}$$

where

$$P = \frac{A_-}{A_+}$$

The error in the radar cross section is  $20 \log_{10} (X_+/A_+)$  and  $20 \log_{10} (X_-/A_-)$ , for fore and aft beam, respectively.

#### Discussion of Theoretical Results

The values of  $20 \log_{10} \frac{X_+}{A_+}$  and  $20 \log_{10} \frac{X_-}{A_-}$  were calculated on a computer (reference 4). The values of  $P$  were taken as 0.01, 0.1, 0.8, 1.0, 10.0, and 100.0. This corresponds to a range of difference of -40 dB to +40 dB between the fore and aft data. Values of  $\theta_e$  were taken as 2.0°, 4.0°, 6.0°, 8.0°, and 10.0°;  $(\alpha+\beta)$  were varied between 0° and 360° in 5° steps. Table II summarizes the results, giving the values of maximum errors. The value of  $(\alpha+\beta)$ , at which the maximum error occurs, is also given in the table. The following conclusions can be drawn from the computed results presented in Table II:

1. The value of maximum error increases as  $\theta_e$  increases and is dependent on the value of  $(\alpha+\beta)$ .

TABLE II.- MAXIMUM VALUE OF ERROR FOR SELECTED PARAMETERS

$\theta_e$ , deg	P	$(\alpha+\beta)$ , deg	$20 \log_{10} \left( \frac{X_+}{A_+} \right)$	$20 \log_{10} \left( \frac{X_-}{A_-} \right)$
2.0	0.01	90	0.00019	8.769
2.0	0.01	270	-0.0028	-2.535
2.0	0.1	90	0.0138	1.395
2.0	0.1	270	-0.0164	-1.666
2.0	0.8	90	0.119	0.186
2.0	0.8	270	-0.12339	-0.1928
2.0	1.0	90	0.14889	0.14889
2.0	1.0	270	-0.15400	-0.15400
2.0	10.0	90	1.395	0.0138
2.0	10.0	270	-1.666	-0.0164
2.0	100.0	90	8.76	0.0001918
2.0	100.0	270	-2.5	-0.002838
4.0	.01	85	-0.00226	13.04
4.0	.01	265	-0.008326	7.926
4.0	0.1	85	0.0249	2.596
4.0	0.1	265	-0.03567	-3.735
4.0	0.8	85	0.2339	0.365
4.0	0.8	265	-0.2513	-0.3929
4.0	1.0	85	0.2928	0.2928
4.0	1.0	265	-0.3139	-0.3139
4.0	10.0	85	0.2596	0.02498
4.0	10.0	265	-3.7353	-0.03567
4.0	100.0	85	13.043	-0.00226
4.0	100.0	265	7.926	-0.00836
6.0	0.01	85	-0.007361	15.8926
6.0	0.01	265	-0.016464	12.5374
6.0	0.10	85	0.03348	3.6479
6.0	0.10	265	-0.05754	-6.4581
6.0	0.80	85	0.3447	0.539159
6.0	0.80	265	-0.38387	-0.60031
6.0	1.0	85	0.4317	0.4317
6.0	1.0	265	-0.4794	-0.4794

TABLE II.- MAXIMUM VALUE OF ERROR FOR  
SELECTED PARAMETERS (Concluded).

$\theta_e$ , deg	P	$(\alpha+\beta)$ , deg	$20 \log_{10} \left( \frac{X_+}{A_+} \right)$	$20 \log_{10} \left( \frac{X_-}{A_-} \right)$
6.0	10.0	85	3.6479	0.03348
6.0	10.0	265	-6.4581	-0.0575
6.0	100.0	85	15.8926	-0.007361
6.0	100.0	265	12.537	-0.016464
8.0	0.01	85	-0.01511	18.032
8.0	0.01	260	-0.02725	15.53
8.0	0.1	80	0.03930	4.5827
8.0	0.1	260	-0.082097	-10.4168
8.0	0.8	80	0.45134	0.70627
8.0	0.8	260	-0.52087	-0.8151
8.0	1.0	80	0.5655	0.5655
8.0	1.0	260	-0.6504	-0.6504
8.0	10.0	80	4.5827	0.03905
8.0	10.0	260	-10.41	-0.08209
8.0	100.0	80	18.032	-0.01511
8.0	100.0	260	15.532	-0.02725
10.0	0.01	80	-0.02551	19.74
10.0	0.01	260	-0.0407	17.75
10.0	0.1	80	0.0425	5.4263
10.0	0.1	260	-0.10944	-18.0867
10.0	0.8	80	0.5544	0.8683
10.0	0.8	260	-0.66337	-1.0390
10.0	1.0	80	0.6953	0.6953
10.0	1.0	260	-0.828	-0.828
10.0	10.0	80	5.426	0.0425
10.0	10.0	260	-18.08	-0.1094
10.0	100.0	80	19.7459	-0.02551
10.0	100.0	260	17.57	-0.04071

2. The value of the error in radar cross section increases as the value of  $P$  becomes small or large compared to 1.0; for example,  $\theta_e = 2.0^\circ$  and  $P = 0.01$ , a maximum error of 8.769 dB can result in the aft beam data.
3. In case the fore and aft data are nearly equal ( $P = 1.0$ ), the maximum error in the value of fore and aft radar scattering cross sections (for  $\theta_e$  up to  $10^\circ$ ) is either 0.695 or -0.828 depending on the value of  $(\alpha+\beta)$ .
4. A computer search was made in order to find the value of maximum error for each value of  $\theta_e$ . This revealed that the value of error in  $\sigma_0$  (fore beam) tends toward -97.95 dB ( $X_+ \rightarrow 0$ ) for the following values of  $\theta_e$ ,  $(\alpha+\beta)$ , and  $P$ .

$\theta_e^\circ$	$(\alpha+\beta)^\circ$	$P$	$X_+/A_+$
1	269.0	114.588	0.2859E - 03
2	268.0	57.29	0.1566E - 03
3	267.0	38.19	0.729E - 04
4	266.0	28.6362	0.555E - 04
5	265.0	22.9037	0.578E - 04
6	264.0	19.0811	0.1265E - 04
7	263.0	16.35	0.3747E - 04
8	262.0	14.300	0.2288E - 04
9	261.0	12.7062	0.2080E - 04
10	260.0	11.4300	0.2677E - 04

Similar results can be obtained for the aft beam case.

5. The error in phase shift due to the ferrite modulator  $\theta_m$  does not affect the radar cross sections.

Comparison of the Theoretical Results  
with Experimental Results

An experimental test was conducted to obtain the value of errors experimentally. The value of the phases was chosen at each frequency so that  $\alpha = \beta = 0$ . The value of  $P$  and  $\theta_e$  can be selected arbitrarily. For the sake of comparison,  $90^\circ$  phase shift is taken as reference on the abscissa in Figure 10. The value of  $P$  is zero, since at this frequency only fore beam data was taken. The computed value of  $X_+/A_+$  for the preceding values of parameters is

$$\frac{X_+}{A_+} = \sqrt{\frac{1 + \cos \theta_e}{2}}$$

The calculated value of  $20 \log_{10} \frac{X_+}{A_+}$  compares extremely well with Figure 10 (of course,  $\theta_e = 0$  corresponds to the  $90^\circ$  point or the no-error point in Figure 10).

Remarks on Phase Error Study

The field scattered by a rough surface at a given point (in a given direction) is necessarily the sum of elementary waves in mutual phase interference. It can be shown that  $\alpha$  and  $\beta$  are uniformly distributed in the range of  $-\pi$  to  $\pi$  (reference 5). Furthermore,  $A_-$  and  $A_+$  are Rayleigh distributed, implying that the maximum errors in the fore and aft scattering cross sections are governed by a probability distribution. Thus, there is a finite probability that the radar cross section has the maximum errors given in Table II.

For the return from sea surfaces, past experimental data and theoretical calculations have shown that the ratio of fore and aft radar cross section is within  $\pm 6$  dB (reference 6). This then would give the value of  $P$  within 0.5 to 2.0. Now, from the calculated values of the maximum error, it can be shown that a maximum error of  $-0.75$  dB can be encountered for the aft or fore beam data, in case  $\theta_e = 4^\circ$ .

It then can be concluded that for the data gathered over ocean, the phase shift error  $\theta_e$  should be maintained to within  $4^\circ$ .

## ANTENNA PATTERN STUDY AND PARAMETRIC EVALUATION

In the data processing plan corresponding to a certain resolution cell geometry (Figure 2), two parameters ( $G_0^2 F'(\theta)$  and  $BW_i$ ) are needed. The antenna gain  $G_0^2 F'(\theta)$  has been calculated in the past as follows:

The maximum value of the product  $G_T(\psi)_\theta G_R(\psi)_\theta$  at any long track angle  $\theta$  is given by  $G_0^2 F(\theta)$ . The integral in equation (2) is evaluated as

$$\int_{-\psi_1}^{\psi_2} G_T(\psi)_\theta G_R(\psi)_\theta d\psi = G_0^2 F(\theta) \cdot \psi(\theta) = G_0^2 F'(\theta) \quad (13)$$

where  $\psi(\theta)$  is the beamwidth between two 3-dB down points at a long track angle  $\theta$ .

To calculate the bandwidths of the filters (the old version of the CAD program), the beamwidth was assumed constant ( $2.5^\circ$ ) and the 3-dB down points symmetrically located with respect to  $\psi = 0$  angle (Figure 11a).

A study of the latest antenna patterns revealed the following factors (reference 7):

1. It is desirable to have all patterns on a digital tape so that the plan for data processing could automatically choose appropriate values of the antenna gain at each incident angle.
2. In order to account for variation of gain along track, a finer grid of the gain along track should be taken. Additionally, the data for  $\sigma_0$  versus  $\theta$  curves should be processed corresponding to those angles where the two-way gain (along track) does not change very rapidly.
3. The maximum gain need not necessarily be on the prime axis. The limits on the skewness of the maximum gain curve should be considered.
4. For patterns where the cross-track beamwidth varies, a variable beamwidth should be included in the computer program.

5. Excessive side-lobes certainly play an important role in the degradation of the final data; therefore, the influence of the side lobes should be considered.
6. The antenna gains are a function of the angles  $\theta$ ,  $\psi$ . Consequently, when the aircraft parameters change, the gain toward a fixed direction changes; thus it is important to consider roll, pitch, drift, and vertical velocity of the aircraft.

To study the preceding factors computer programs were developed. A tape first was generated on which two-way gains were recorded. The tape was generated by multiplying the antenna gains of the transmitting and receiving antennas. The beamwidths, bandwidths, and antenna gains were computed from the tape using computer programs. The values for two-way antenna patterns were taken in increments of  $0.2^\circ$  in the long track angle. The results (reference 8) are summarized below.

#### Redop 1 Modified Antenna Patterns

The effect of Redop 1 modified antenna patterns is demonstrated by computing the factor  $10 \log_{10} \left( \frac{1}{BW_i} \right)$  and  $G_0^2 F'(\theta)$ . The value of  $(BW_i)$  is given by Figures 11b and 11c

$$BW_i \approx \frac{2VL}{\lambda h} \cos^3 \theta \cos \frac{\Delta\theta}{2} \quad (14)$$

First, the value of  $BW_i$  was calculated using the old pattern (reference 1) values and the parameters

$$h = 3000 \text{ feet}$$

$$V = 200 \text{ knots}$$

The area illuminated for each resolution cell = 22,500 square feet. Then, using the same parameters as before, Redop 1 modified patterns were used for calculation of equation (14). The results are shown in Figure 12.

The beamwidth  $\psi(\theta)$  and gain  $G_0^2 F'(\theta)$  are shown in Figures 13 and 14. These computations were completed as outlined in equation (13). These figures outline the significant differences between the old pattern and the Redop 1 modified.

### Long Track Antenna Gain Variations

In order to study the effect of long track antenna gain variation and side-lobe effects, three types of integrations were performed:

The 3-dB Summation Method.- In this case the maximum value of two-way gain ( $G_0^2 F(\theta)$ ) was determined at an angle  $\theta$ . From  $G_0^2 F(\theta)$  dB, a 3-dB value was subtracted. Two values of  $\psi$  ( $\psi_1$  and  $\psi_2$ ) were determined where gain equaled ( $G_0^2 F(\theta) - 3$  dB). The 3-dB summation beamwidth is defined by

$$\psi_{3s}(\theta) = \frac{\sum_{\psi_1}^{\psi_2} G_0^2 F(\theta) f(\theta, \psi) \Delta\psi}{G_0^2 F(\theta)} \quad (15)$$

In equation (15),  $G_0^2 F(\theta)$  is expressed in numerical value and not in dB. The increments are taken as  $0.5^\circ$ . The gain corresponding to this beamwidth is given by

$$\left[ G_0^2 F'(\theta) \right]_{3s} = G_0^2 F(\theta) + \psi_{3s}(\theta) \quad (16)$$

where quantities are expressed in dB.

Summation Method.- A rearrangement of equation (2) led to the following result

$$\sigma_0(\theta, \psi = 0) = \frac{2P_r V(4\pi)^3 h^2}{P_T G_0^2 f(\theta) \lambda^3 \Delta f_d \int_{\psi} f(\theta, \psi) f_{\sigma}(\theta, \psi) d\psi} \quad (17)$$

where

$$f_{\sigma}(\theta, \psi) = \frac{\sigma_0(\theta, \psi)}{\sigma_0(\theta, \psi = 0)}$$

For a constant incidence angle approximation, all points on a constant doppler have incidence angles equal to  $\theta$  at the point where the doppler line crosses  $\psi = 0$ . Based on the above assumption

$$\int_{\psi} f(\theta, \psi) f_{\sigma}(\theta, \psi) d\psi = \int_{\psi} f(\theta, \psi) d\psi \approx \psi(\theta)_S$$

The above equation can be written as

$$\psi(\theta)_S = \sum f(\theta, \psi) \Delta\psi \quad (18)$$

An equivalent expression of equation (18) used to evaluate the "equivalent" beamwidth  $\psi(\theta)_S$  from the tabulated results is given by

$$\psi(\theta)_S = \frac{\sum G_0^2 F(\theta) f(\theta, \psi)}{G_0^2 F(\theta)} \Delta\psi \quad (19)$$

where the summation is taken over  $-10^\circ \leq \psi \leq 10^\circ$ .

Since by definition  $G_0^2 F'(\theta)$  is the product of the two-way antenna gain times the integral of the port-starboard beamwidth for any incidence angle, the two-way gain is computed as follows

$$\left[ G_0^2 F'(\theta) \right]_S = G_0^2 F(\theta) \cdot \psi(\theta)_S \quad (20)$$

In equations (19) and (20) the quantities are taken in numerical value.

Cumulative Power at 95 Percent.- The following analysis was conducted to determine the overall effect of the antenna side-lobes on resolution (reference 8):

- Evaluate the total area under the curve (as shown in Figure 15a) as a function of cross-track angle  $\psi$  for angular lengths  $\pm\Delta\psi$  at each incident angle  $\theta$ .
- From the digital results of the computed two-way cross-track antenna gains given for incidence angles of  $-70 \leq \theta \leq +70^\circ$  and cross-track angles of  $-10 \leq \psi \leq +10^\circ$ , the specific two-way beamwidth can be calculated as follows:
  - (1) For specific  $\theta$  convert the digital cross-track gains which are given for  $\pm\psi$  values up to  $10^\circ$  to their decimal representation; i.e.,  $N = 10^{\text{dB}/10}$ .
  - (2) Integrate the energy area obtained using the converted  $N$  values by using Romberg's integration technique. See Figure 15a for an illustrative ideal example of the areas to be integrated.
- Plot the areas found by the above integrations. (Plot: Percent of Cumulative Cross-Track Beam Power vs Cross-Track Angle.)
- Normalize the values with the maximum value (Figure 15b).
- From the above plot determine the two-way beamwidth value  $\psi(\theta)_c$  at 95 percent power point.
- Find  $G_0^2 F'(\theta)$  using the new calculated two-way beamwidth values; i.e.,  $G_0^2 F'(\theta) = G_0^2 F(\theta) + \psi(\theta)_c$  in dB.

The results of the computer-generated programs are summarized in Figures 16 and 17. These graphs can be utilized in the CAD computer processing plan. The selection of angles at which  $\sigma_0$  should be computed also can be made on the basis of these graphs.

#### Aircraft Parameters

Errors caused by aircraft parameter changes (vertical velocity, roll, pitch, and yaw) can be introduced into the processed data. Examples are given below to illustrate this point.

Vertical Velocity.- First, it is assumed that the aircraft has a ground speed (horizontal)  $V$  of 200 knots. With the following parameters, incident angle  $\theta$  is calculated

$$h = 3000 \text{ feet}$$

$$L, \text{ length in long track of} \\ \text{each resolution cell} = 150 \text{ feet}$$

As a second step, in addition to the preceding aircraft parameters, a vertical velocity  $V_z$  of 10 knots is assumed. The incident angle corresponding to the new parameters is given by

$$\theta_1 = \sin^{-1} \left[ \frac{\lambda f_d}{2V} \right] + \tan^{-1} \left[ \frac{V_z}{-V} \right] \quad (21)$$

If the antenna gain is not taken at  $\theta_1$  angle in the presence of vertical velocity, the error caused by improper antenna gain is

$$G_0^2 F'(\theta_1) - G_0^2 F'(\theta)$$

This error is listed in Table III.

Roll.- The effect of roll (Figure 18) is to change the incident angle to

$$\theta_2 = \cos^{-1} \left[ \cos \theta \cos \xi \right] \quad (22)$$

First, we assume the parameters are given in the example above (vertical velocity = 0). Then a roll ( $\xi$ ) of  $4^\circ$  is introduced and  $\theta_2$  is calculated. The error caused by improper gain inclusion in the processing plan is

$$\left[ G_0^2 F'(\theta) - G_0^2 F'(\theta_2) \right]$$

TABLE III.- VERTICAL VELOCITY ERROR

<u><math>\theta</math></u> (Fore beam, degrees)	<u><math>\theta_1</math></u>	<u>Error due to</u> <u><math>V_z = 10</math> knots</u> <u>(dB)</u>
2.5	-0.36	0.69
5.0	2.1	0.65
10.0	7.1	1.78
15.0	12.1	0.25
20.0	17.1	1.50
25.0	22.1	0.50
30.0	27.1	1.97
35.0	32.1	1.70
40.0	37.1	1.62
45.0	42.1	0.51
50.0	47.1	1.90
55.0	52.1	1.50
60.0	57.1	0.37

Table IV presents these errors

TABLE IV.- ERROR CAUSED BY ROLL OF 4°

$\theta$ (Fore beam, degrees)	$\theta_2$	Error due to $\xi = 4^\circ$
2.5	4.71	0.59
5.0	6.4	0.38
10.0	10.76	0.42
15.0	15.51	0.27
20.0	20.38	0.11
25.0	25.29	0.25
30.0	30.24	0.23

Pitch and Yaw.- Pitch variations can be treated in the same manner as roll variations. In the present processing program the pitch corrections are taken automatically. Yaw errors are minor for small yaw changes over water. Procedures for taking into account roll and vertical velocity are being investigated. However, MSC is attempting to screen the flight parameter data and not process data where these parameters are excessive.

## DATA PROCESSING

Scatterometer data can be processed by either analog or digital processing programs. There are several advantages in processing the data on a digital computer. In the past, questions have been raised as to the consistency between analog and digital processed data. A review of analog and digital programming capabilities was undertaken to investigate all anomalies. A summary of the results follows:

### TEST TAPE STUDY

A test tape was generated using analog equipment with known amplitudes. The data recorded consisted of a basic 400 Hz square wave complete with harmonics on one track of the test tape and the same signal shifted by 90° (lagging) on the second track. This tape was processed with both analog and digital equipment. The filter bandwidths were chosen properly (reference 9). For frequencies (harmonics) up to 2 kHz (5th harmonic), good comparison between analog and digital results was observed. The differences at higher frequencies were attributed to the azimuth alignment of the tape recorder read heads. The alignment error was eliminated later by introducing an adjustment routine.

Further study was done using another tape (reference 10). The signals recorded on the tape were made similar to the scatterometer return from a typical ocean surface. It was shown that a change of 4.24 dB was introduced by hamming the data on the digital computer. The digitally generated tape was converted to analog data and processed by analog equipment. The analog and digital results compared very well.

### NOISE FLOOR LEVEL

In the process of comparing analog and digital filtered data, it was noted that the analog processing presented a noise floor of -70 dB while the digital filtering could produce no better than -55 dB (Figure 19). An investigation revealed that some of the high-frequency noise was being folded back into the data in the digital filtering. Additionally, the data were not being processed properly to realize full resolution of the calibration signal versus data. The program now has equipment and procedures incorporated to reduce these effects. The change incorporated was the utilization of Redcor filters to reduce the high-frequency noise power component. The amplification

of data to band edge enabled increased resolution of the data. Data now processed with digital equipment present a noise floor near -70 dB (Figure 20).

#### Effect of Gain Variations

In reviewing past data (Flight 6, Mission 88) it was found that a large change in reference signal had taken place with a channel gain change in the system. Furthermore, it was found that the reference signal was not being continuously monitored in the computer program. Thus, a jump in the data was noticed corresponding to the gain change. Two steps were taken to alleviate this problem:

- The data processing program monitors both data and reference signal throughout a given flight line.
- A gain change should be avoided during a given flight line.

In reviewing Mission 88, Flight 6 data after the program modification, it was apparent that no jump in the data because of channel gain change existed.

#### Data Averaging Errors

In reviewing the past processed data it was noticed that the computer program was computing the statistical average of  $\sigma_0$  by averaging the dB values rather than the numerical value  $N$  of the scattering cross section. To correct this, first the value of scattering cross section was calculated as a number, then averaged, and the average was expressed in dB.

#### Aircraft Parameter Errors

In the program for processing the data, proper values of  $h$ ,  $V$ ,  $V_z$  must be taken for each instant of time. As an example, if  $V$  changes by 10 knots, the bandwidth of the filters changes. This is illustrated in Figure 21 for the following parameters:

$$V_1 = 200 \text{ knots}$$

$$V_2 = 210 \text{ knots}$$

$$\Delta\theta \text{ (constant)} = 3^\circ$$

$$h = 3000 \text{ feet}$$

where  $V_1, V_2$  are the aircraft velocity and  $\Delta\theta$  the resolution cell angle. Similarly, altitude and vertical velocity ( $V_z$ ) changes can cause errors in the processed data. In the processing plan currently used, altitude, aircraft velocity  $V$  and pitch variation are properly accounted for.

REFERENCES

1. Scatterometer Data Analysis Program, Final Report, No. 57667-2, Ryan Aeronautical Company, September 1967.
2. Program Documentation, Scatterometer Filter Program (FILT13), Program Q605, Project 4610, prepared for Computation and Data Analysis Division, NASA/MSC, February 1970.
3. Jordan, L., Interdepartmental Communication, LEC No. 71-015-PCN-97, to G. Graybeal, May 1970.
4. Krishen, K., Interdepartmental Communication, LEC No. 71-015-PCN-109, to G. Graybeal, June 1970.
5. Beckmann, P. and Spizzichino, A.; The Scattering of Electromagnetic Waves From Rough Surfaces; The MacMillan Company, New York, 1963.
6. Krishen, K., Saturation of  $\sigma_0$  With Increasing Wind Velocity, Technical Report No. 649D.21-007, Lockheed Electronics Company, Houston, August 1969.
7. Krishen, K., Definition of Scatterometer Antenna Problems and Possible Approaches to Data Processing, Technical Report No. 649D.21.011, Lockheed Electronics Company, Houston, December 1969.
8. Vlahos, N. and Kell, T., Study of Antenna Patterns and Parametric Evaluation for 13.3-GHz Single Polarization Radar Scatterometer, Technical Report No. 649D.21.030, Lockheed Electronics Company, Houston, November 1970.
9. Vlahos, N., Analysis of Analog vs Digital Filtering Techniques as Applied to Radar Scatterometry, Technical Report No. 649D.21.032, Lockheed Electronics Company, Houston, July 1970.
10. Krishen, K., Preliminary Evaluation of Computation and Analysis Division (CAD) 13.3-GHz Single Polarized Scatterometer Data Processing Program, Interdepartmental Communication, LEC No. 78-015-PCN-06, to B. Baker (NASA/MSC), October 1970.

613

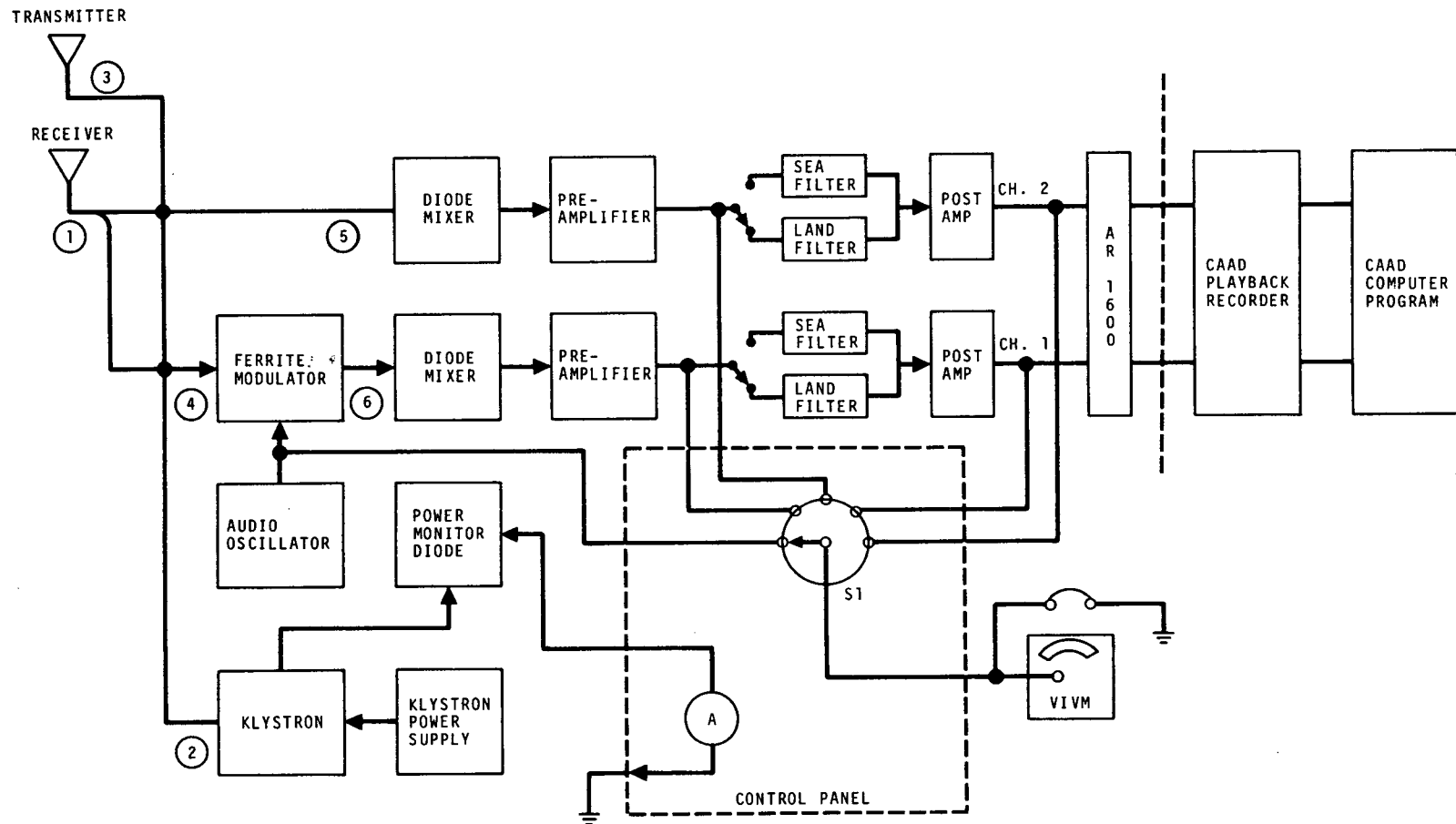


Figure 1. - 13.3 GHz scatterometer system block diagram.

614

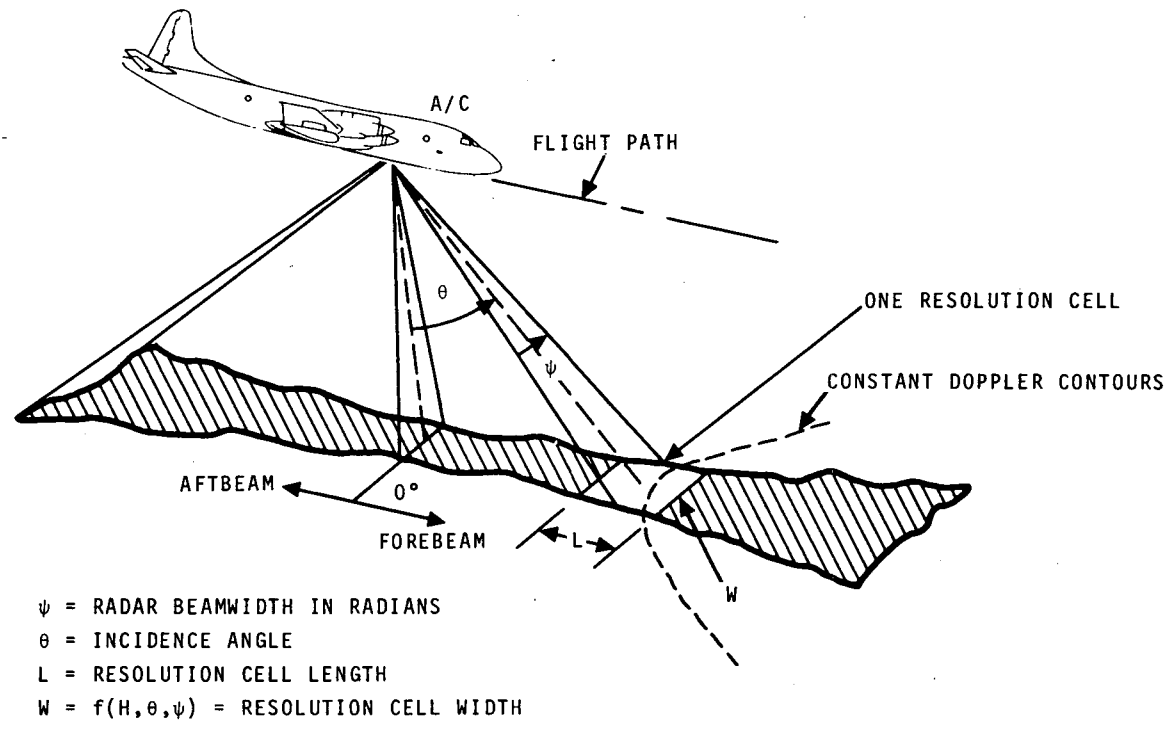


Figure 2. - 13.3 GHz scatterometer, resolution cell geometry.

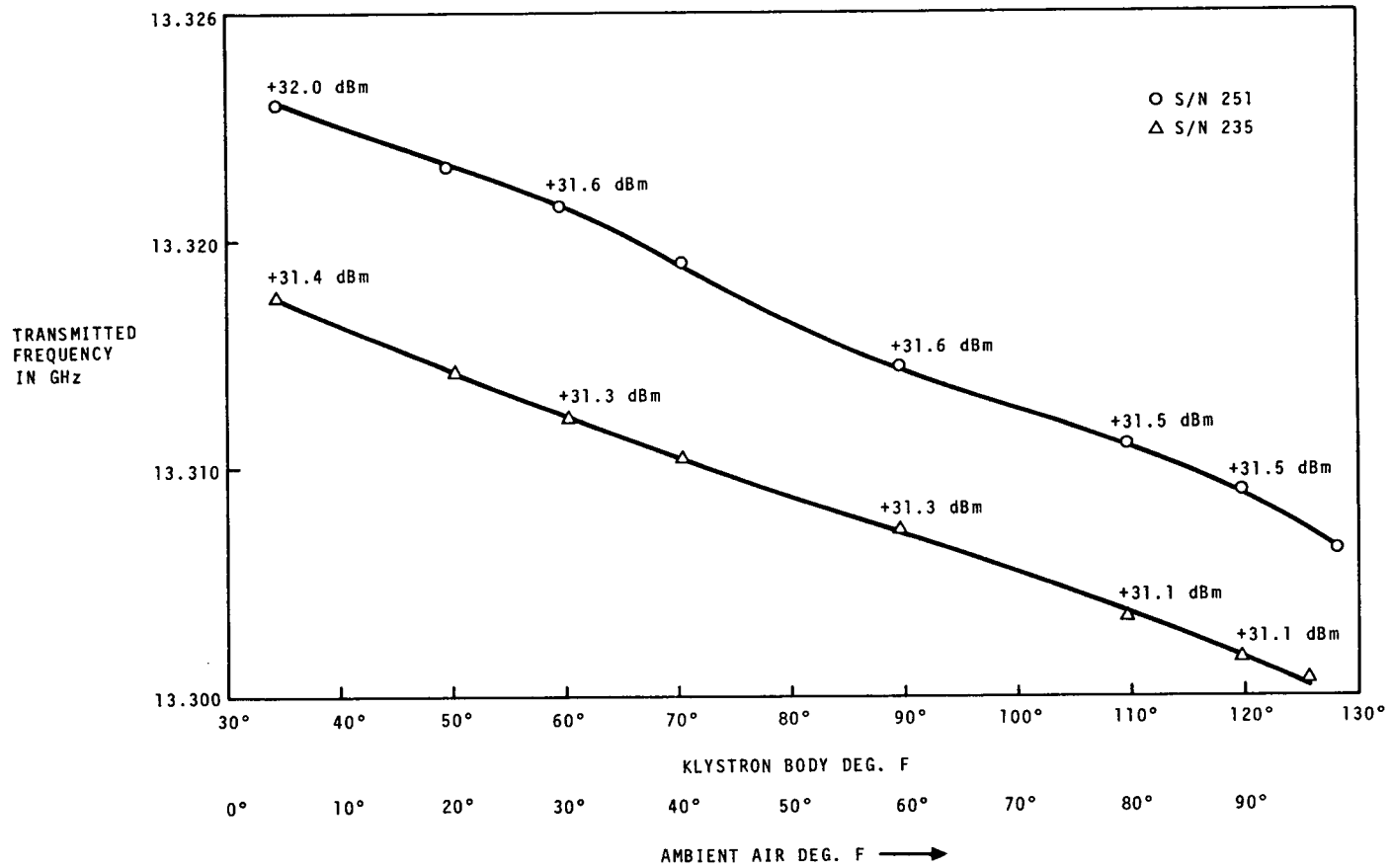


Figure 3. - Klystron temperature stability

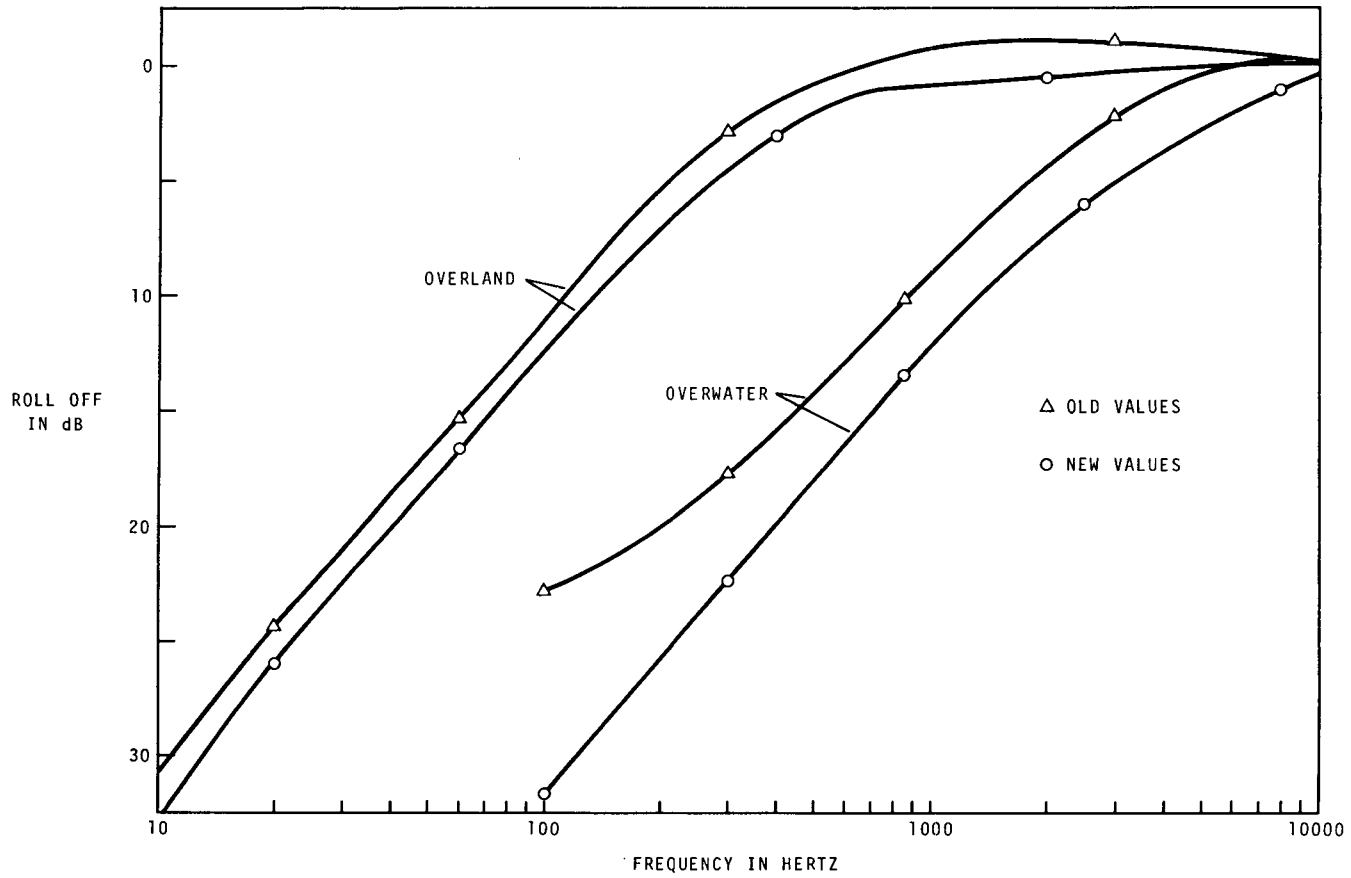


Figure 4. — Rolloff values for 13.3 GHz scatterometer.

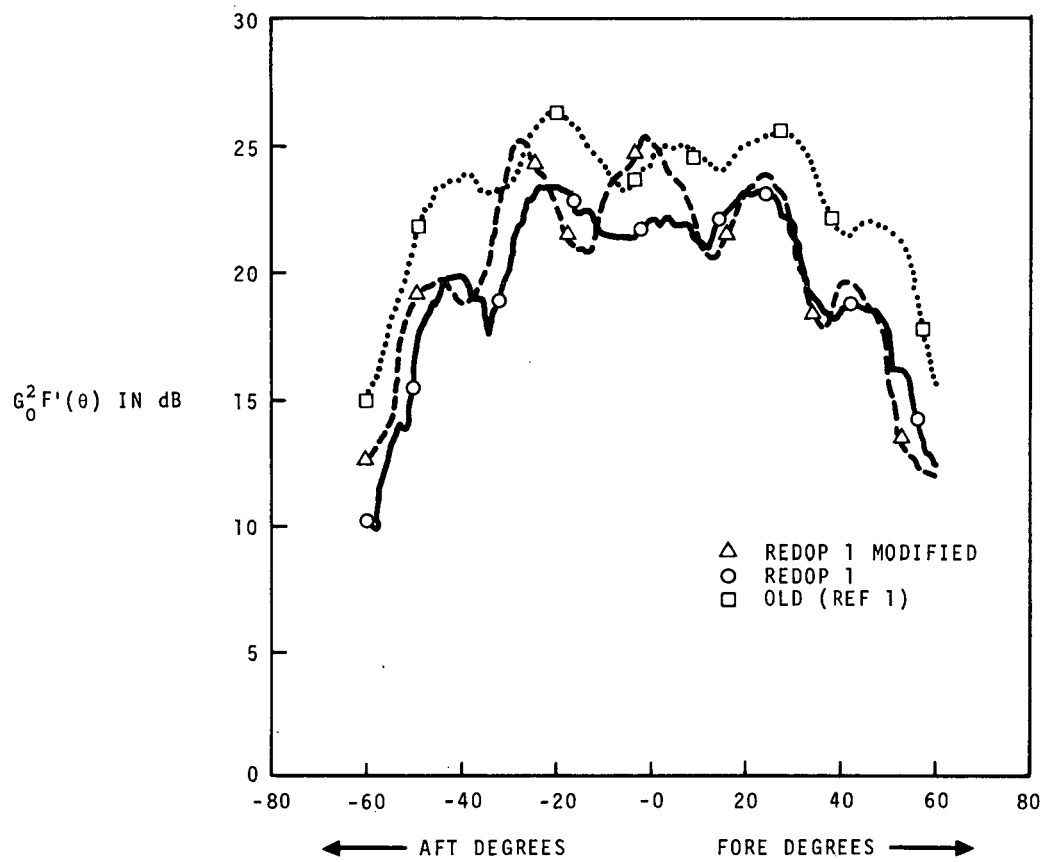
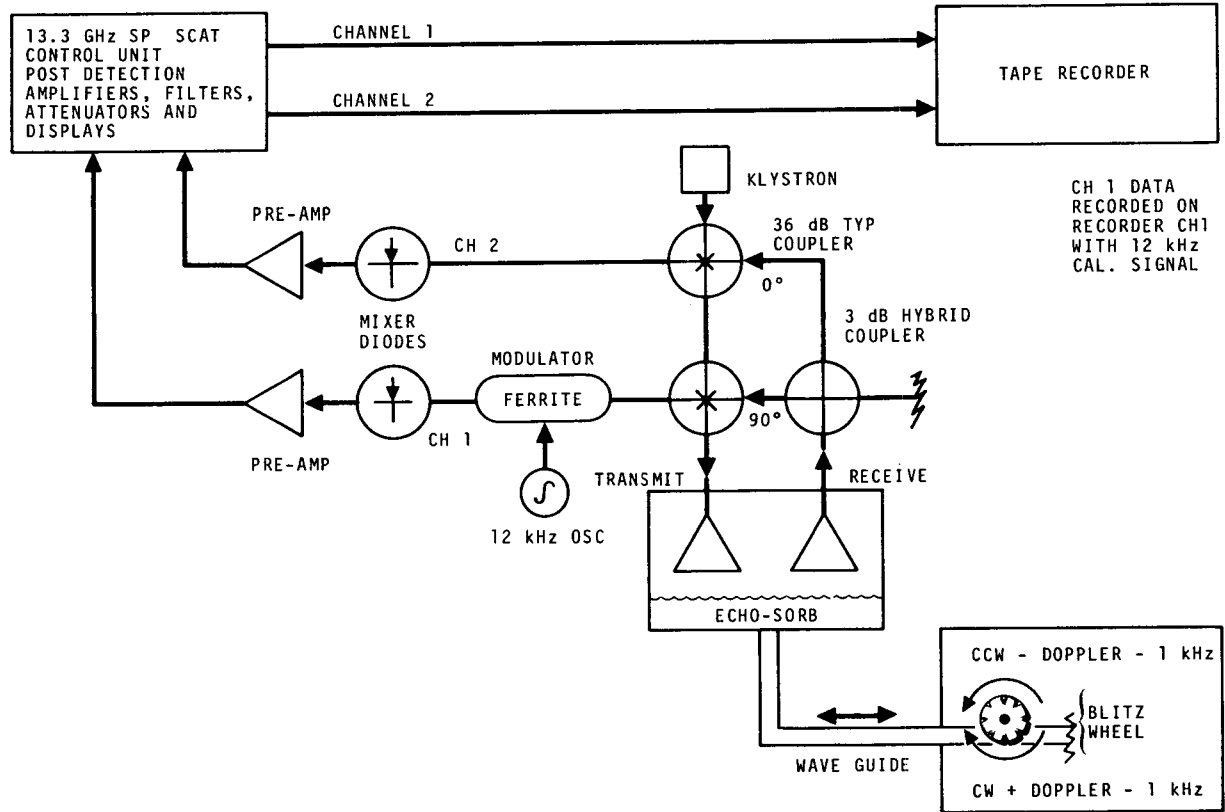


Figure 5. —  $G_0^2 F'(\theta)$  values with 3dB beamwidth.

618



CH 1 DATA RECORDED ON RECORDER CH1 WITH 12 kHz CAL. SIGNAL

Figure 6. - 13.3-GHz Single Polarized Scatterometer blitz wheel test.

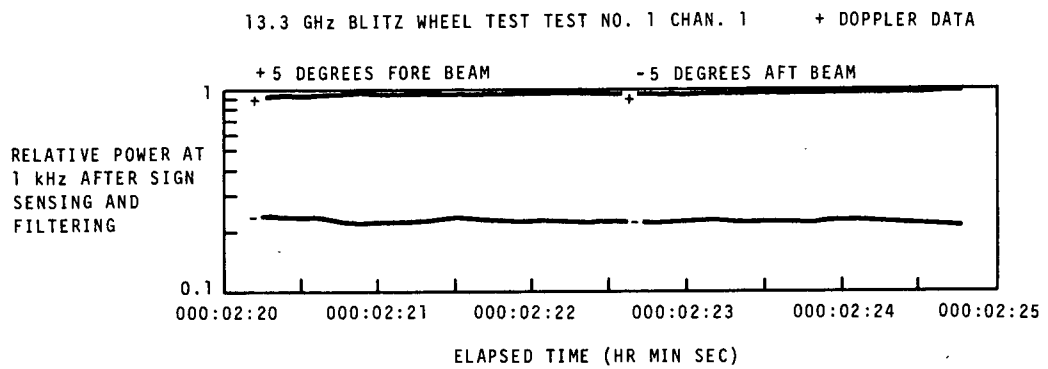


Figure 7. — Digital program output of the blitz wheel test.

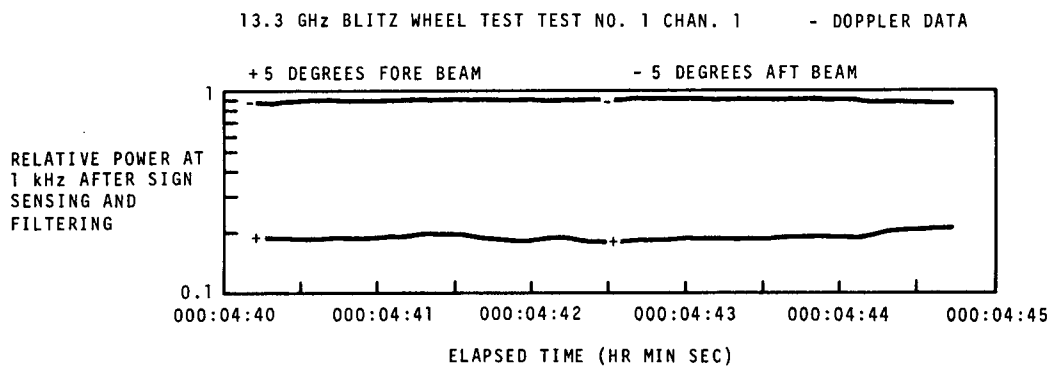


Figure 8. — Digital program output of the blitz wheel test.

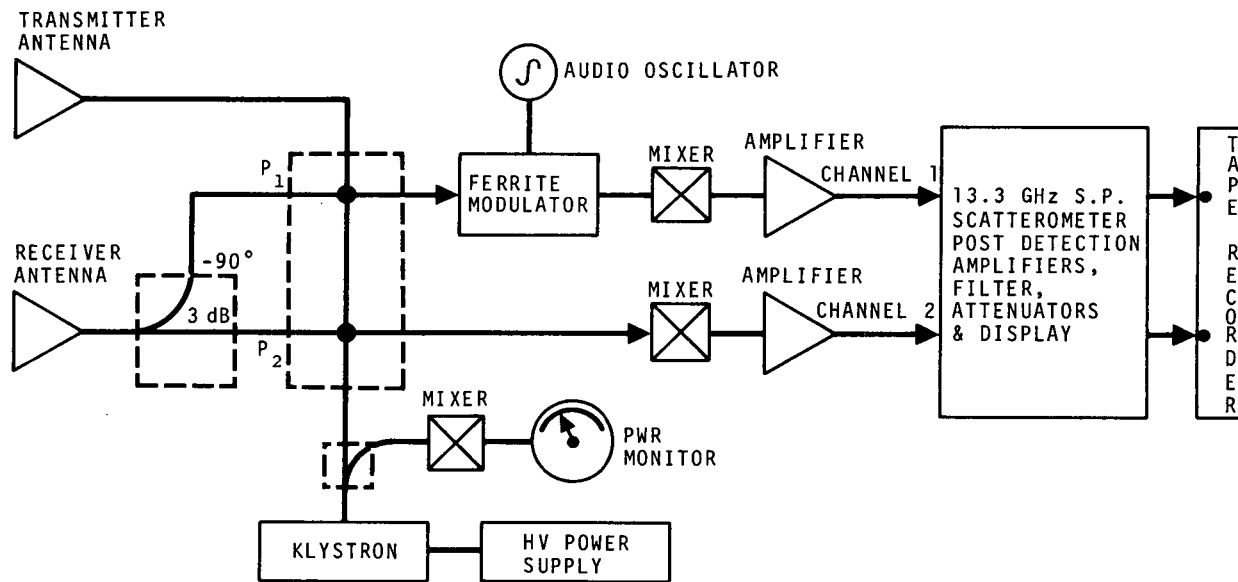


Figure 9. - 13.3 GHz single polarized scatterometer diagram showing channel phase shift.

621

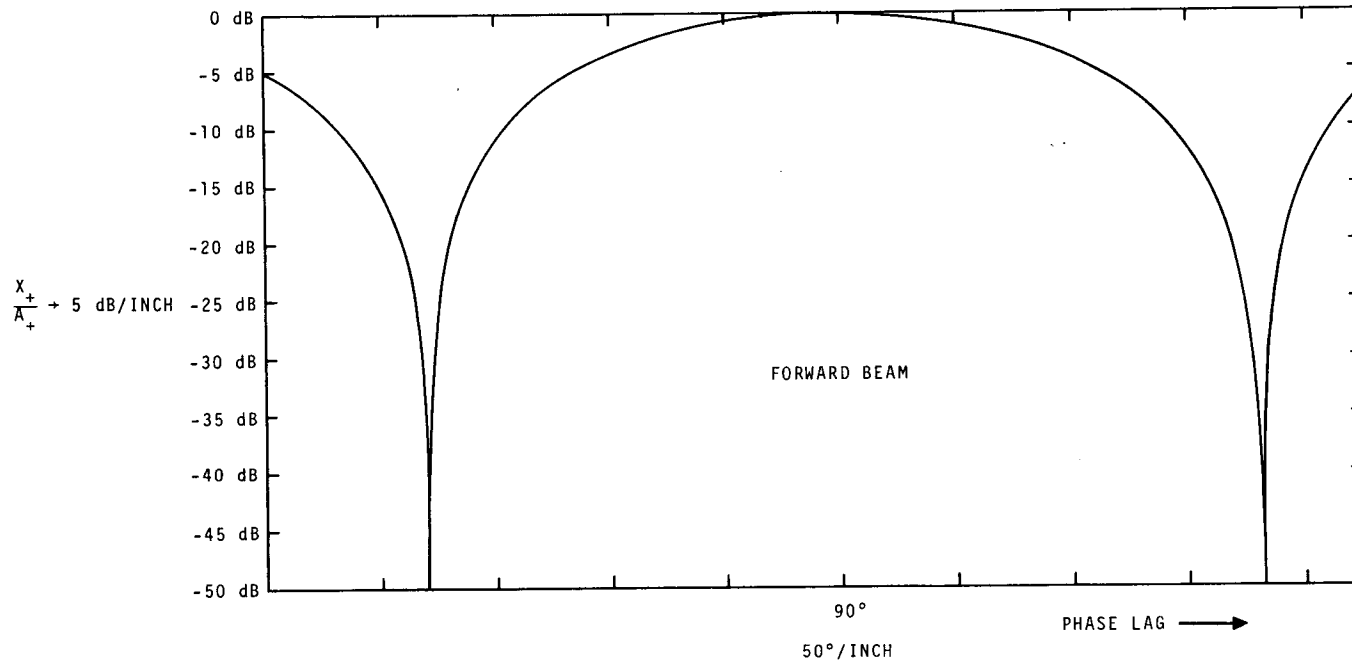


Figure 10. — Experimental results of phase shift study.

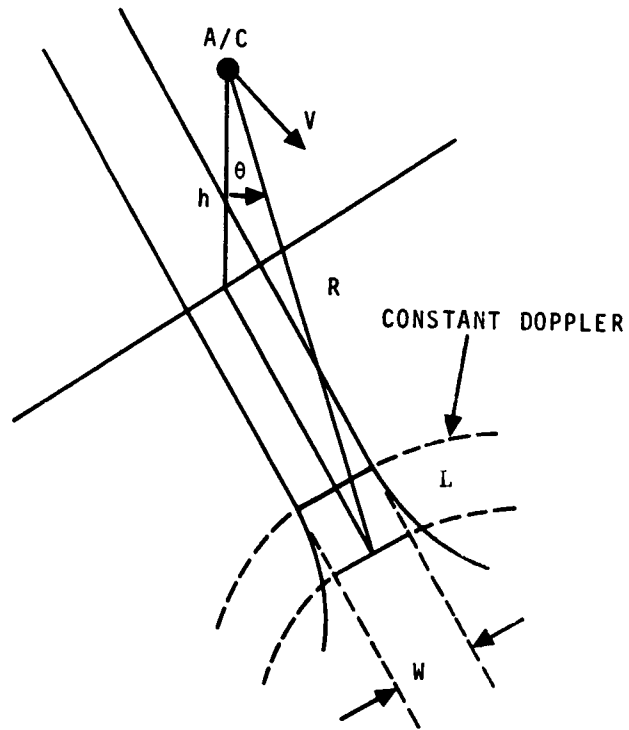


Figure 11a. - Resolution cell geometry.

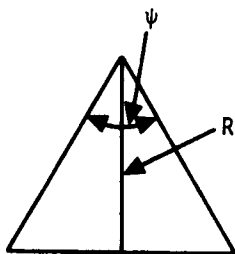


Figure 11b. - Cross track geometry.

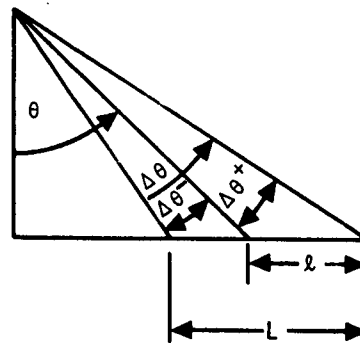


Figure 11c. - Along track geometry.

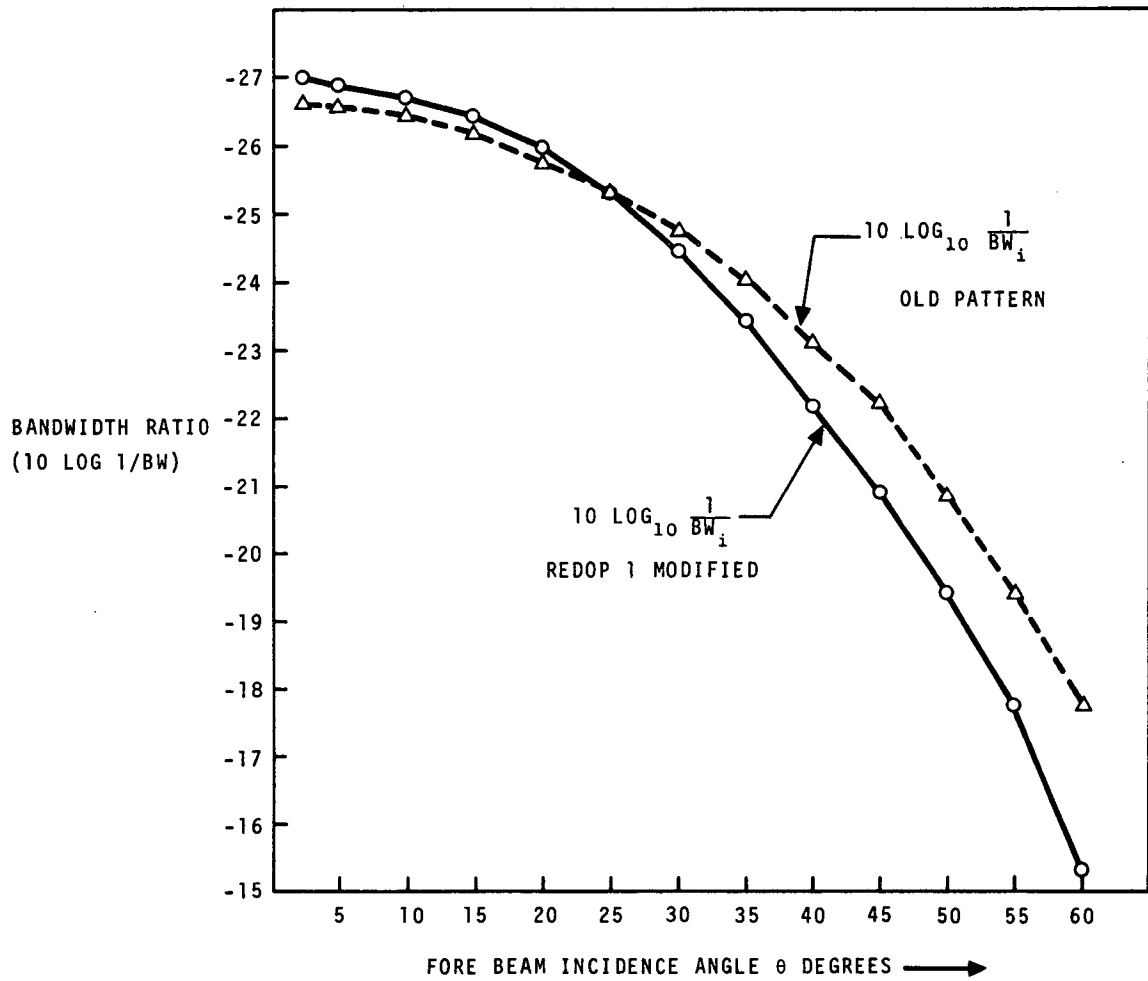


Figure 12. - Cross-section ratio of bandwidths.

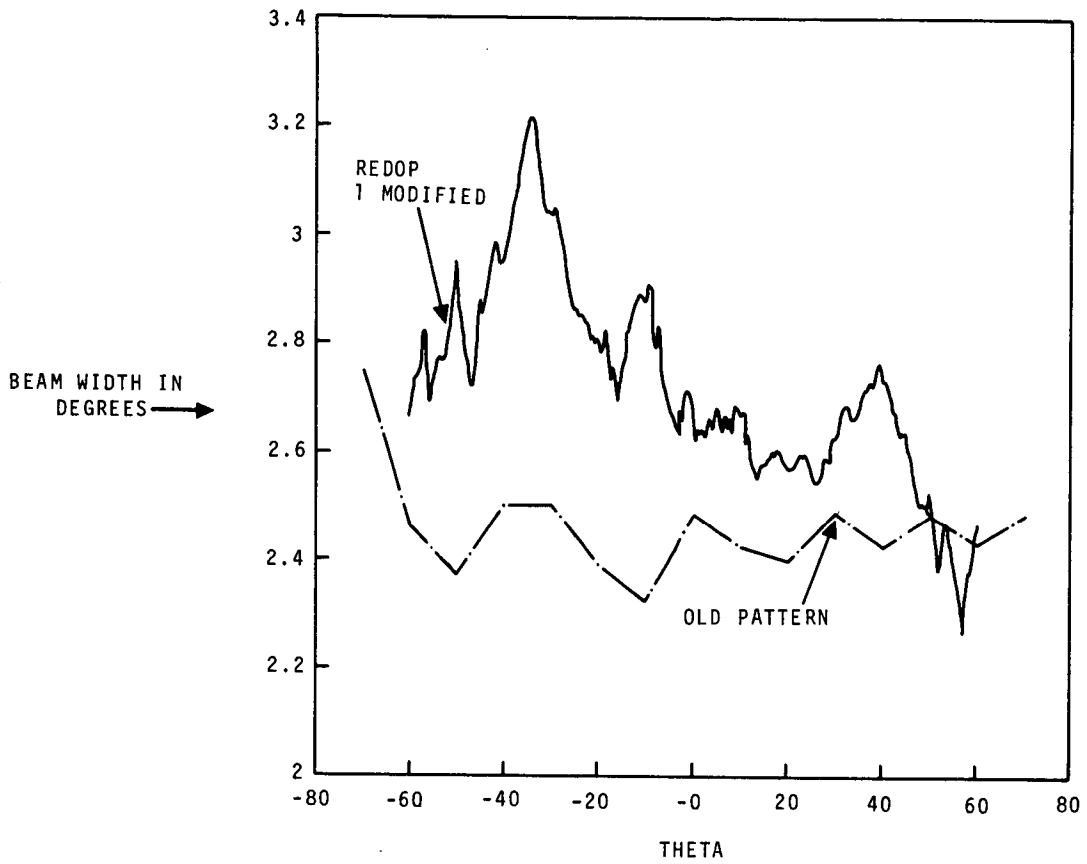


Figure 13. - Comparison of old and Redop 1 modified beamwidths computed according to equation (13).

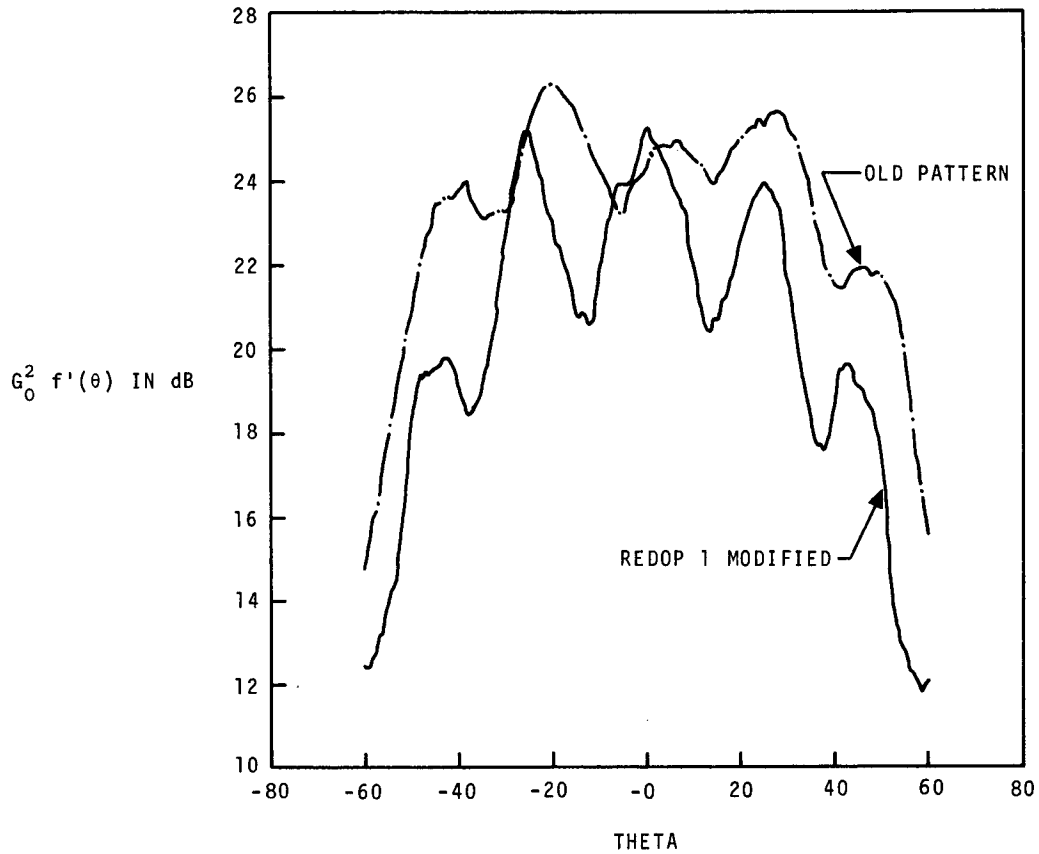


Figure 14. - Comparison of antenna gains  $G_0^2 F'(\theta)$  of old and Redop 1 modified antenna patterns computed according to equation (13).

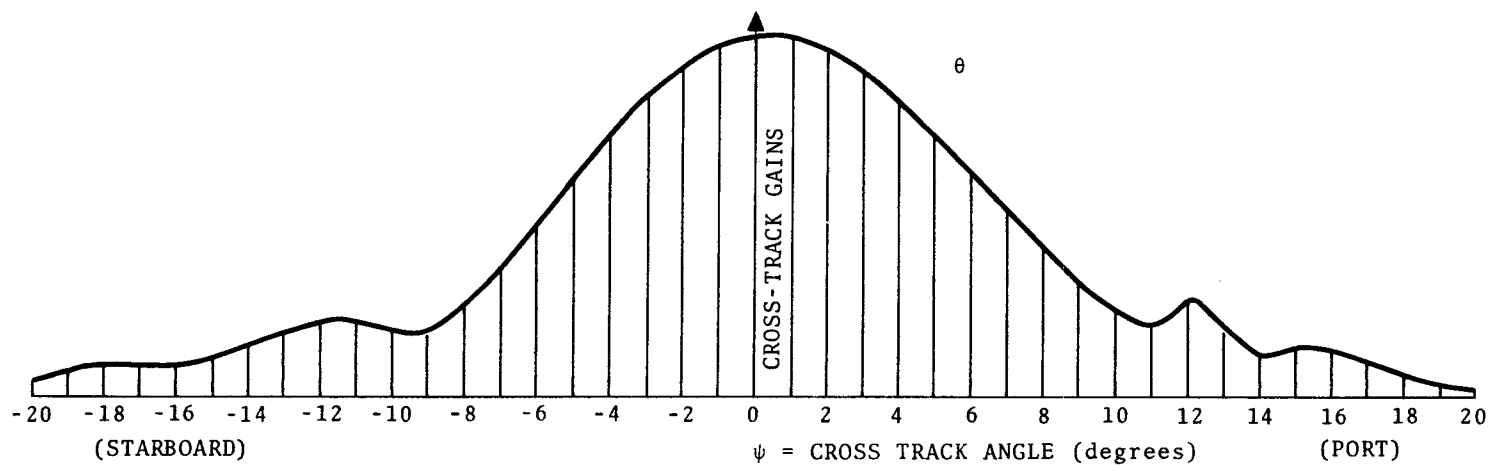


Figure 15a. — Area of total transmitted/received antenna energy

626

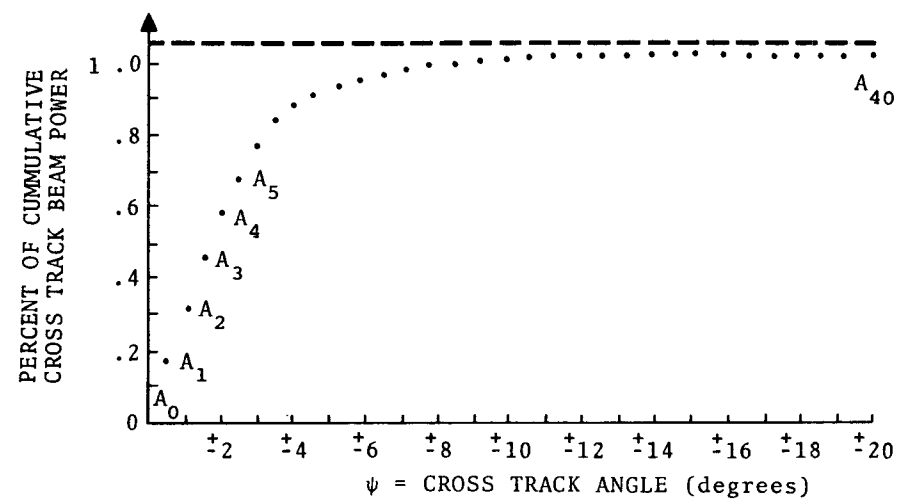


Figure 15b. — Cumulative probability (percent of total power)

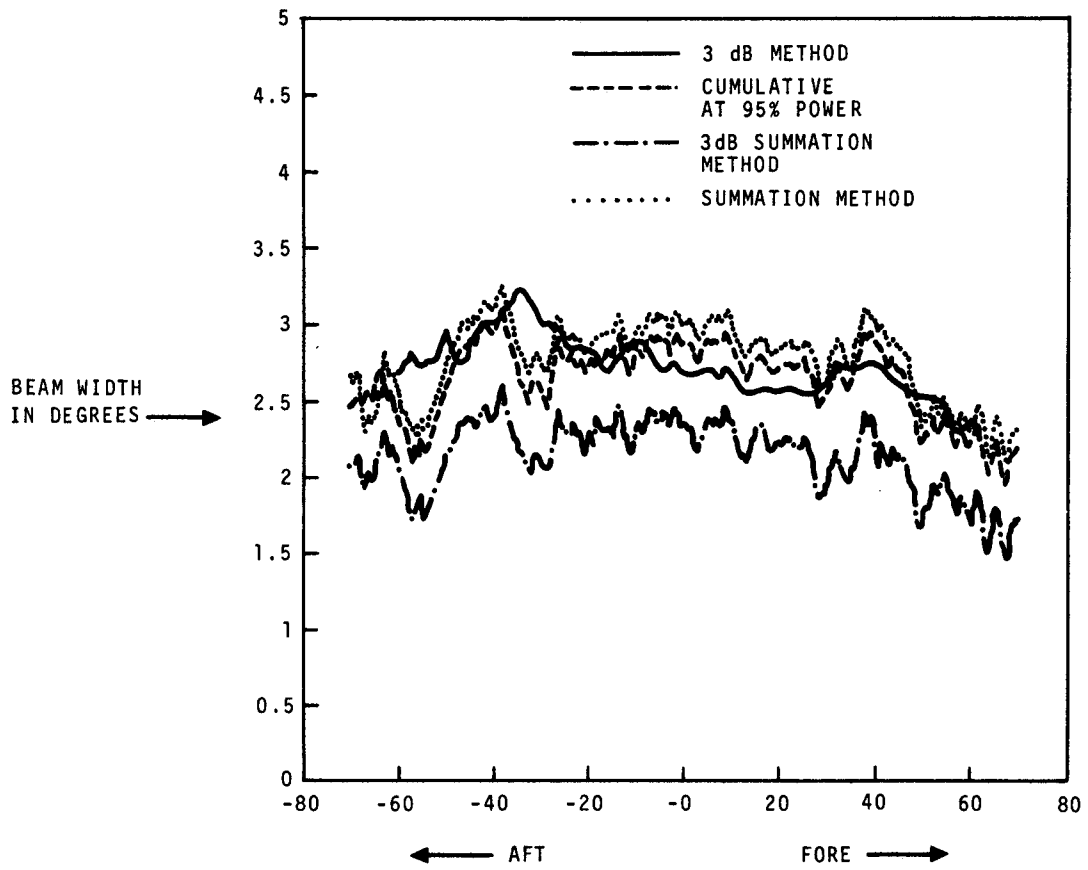


Figure 16. - The value of beamwidth using various methods for Redop 1 modified antenna patterns.

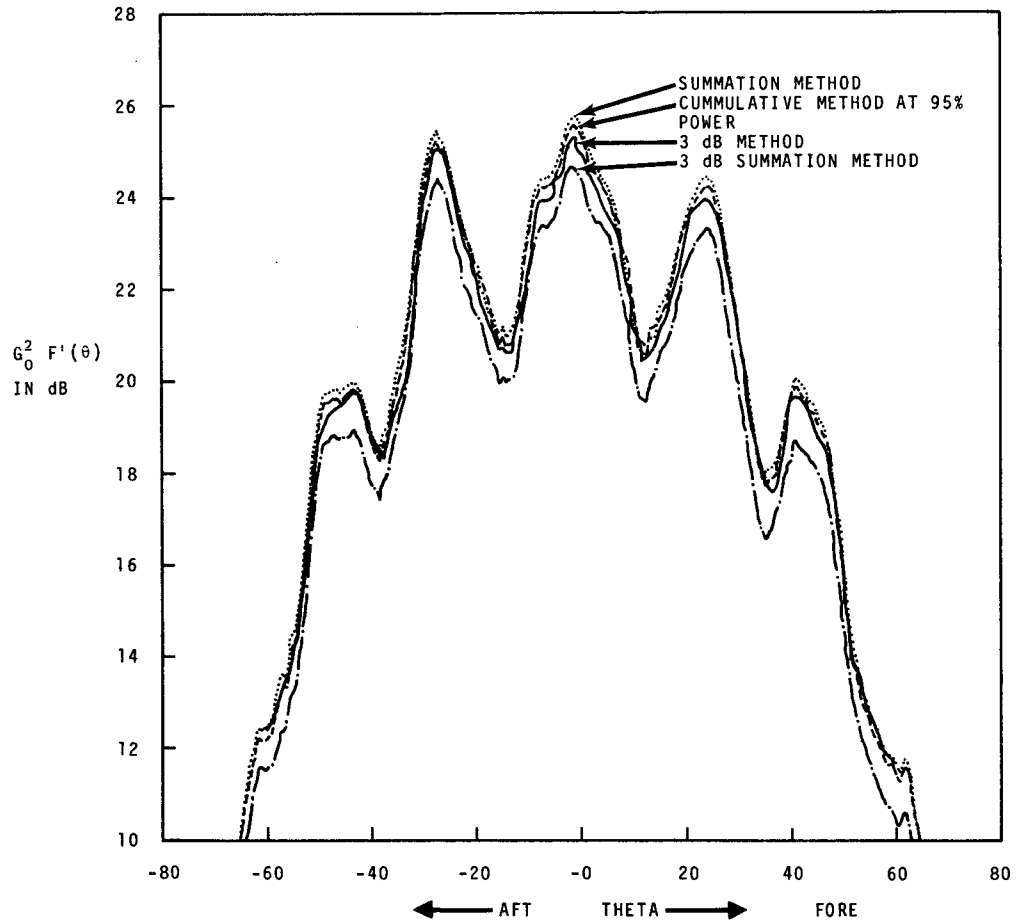
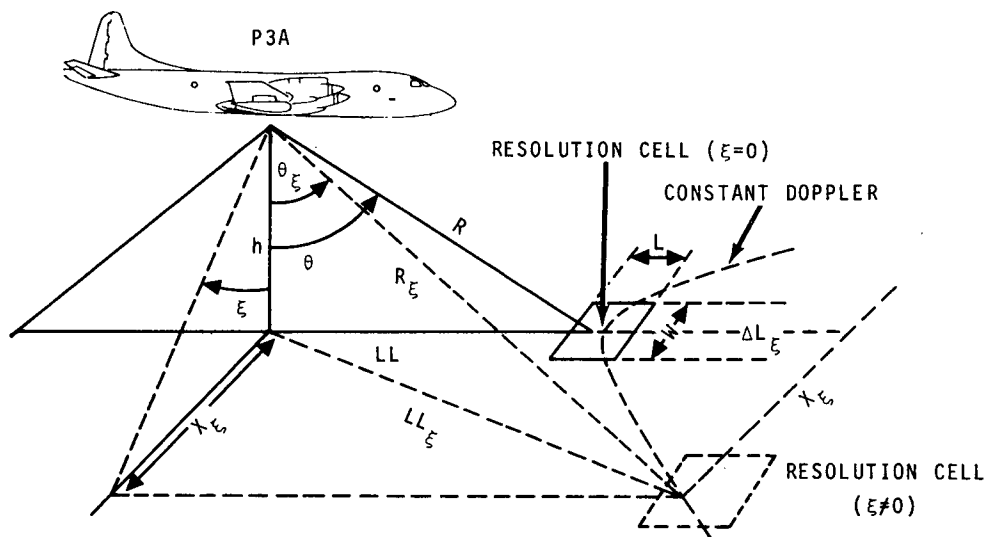


Figure 17. — The value of  $G_0^2 F'(\theta)$  using various methods for Redop 1 modified antenna patterns



- $\epsilon$  = ROLL ANGLE
- $\theta_\epsilon$  = NEW INCIDENCE ANGLE IN THE PRESENCE OF ROLL ANGLE
- $R$  = SLANT RANGE FROM ANTENNA TO RESOLUTION CELL CENTER
- $R_\epsilon$  = SLANT RANGE FROM ANTENNA TO RESOLUTION CELL CENTER WITH ROLL ANGLE
- $W$  = RESOLUTION CELL WIDTH
- $L$  = RESOLUTION CELL LENGTH
- $LL$  = LOCATION OF RESOLUTION CELL
- $LL_\epsilon$  = DISTANCE AWAY FROM FLIGHT LINE
- $\Delta L_\epsilon$  = ALONG TRACK DISPLACEMENT

Figure 18. — Resolution cell geometry in the presence of roll variation

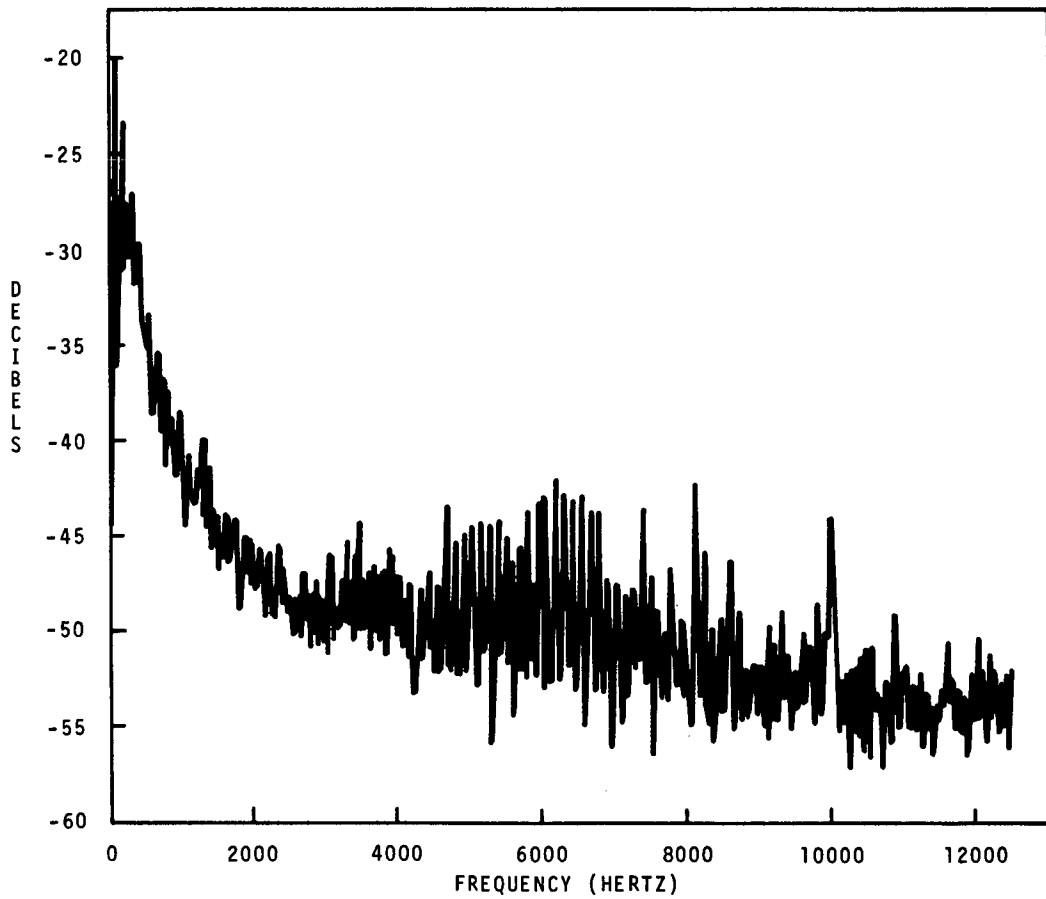


Figure 19. - Typical digital computer processed data plot (PSD) for Mission 119 (FCF) before program change.

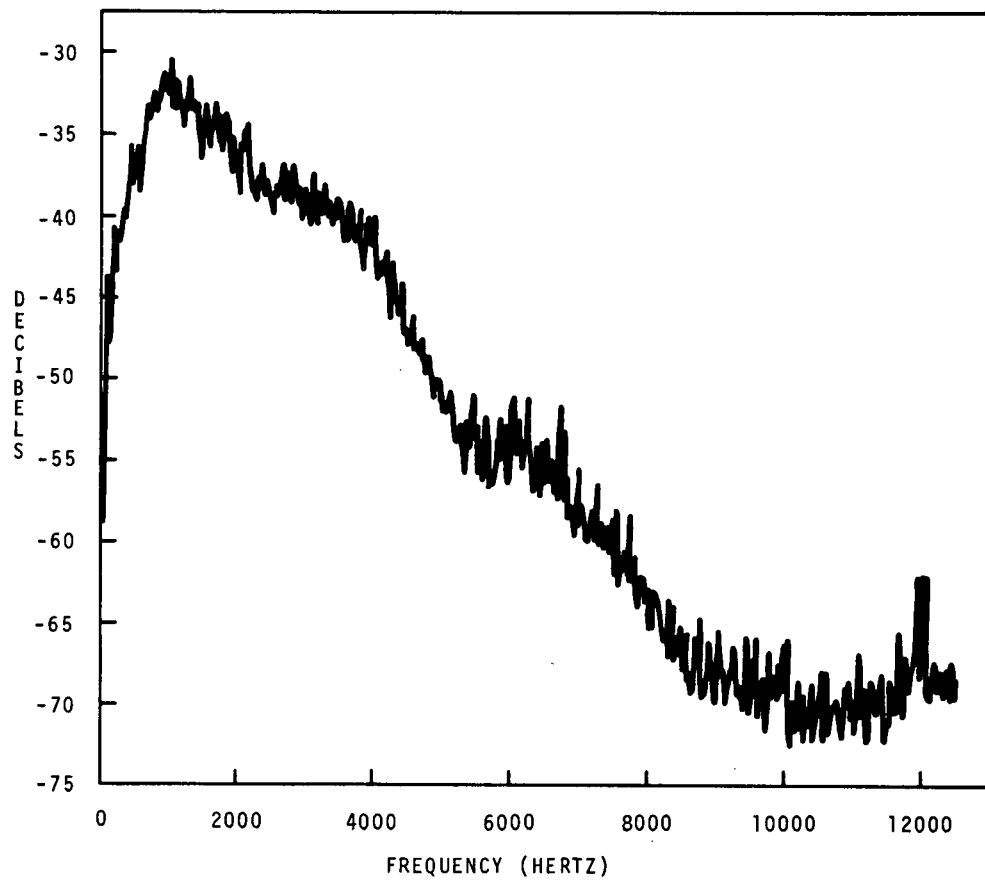


Figure 20. - Typical digital computer processed data plot (PSD) for Mission 119 after program change.

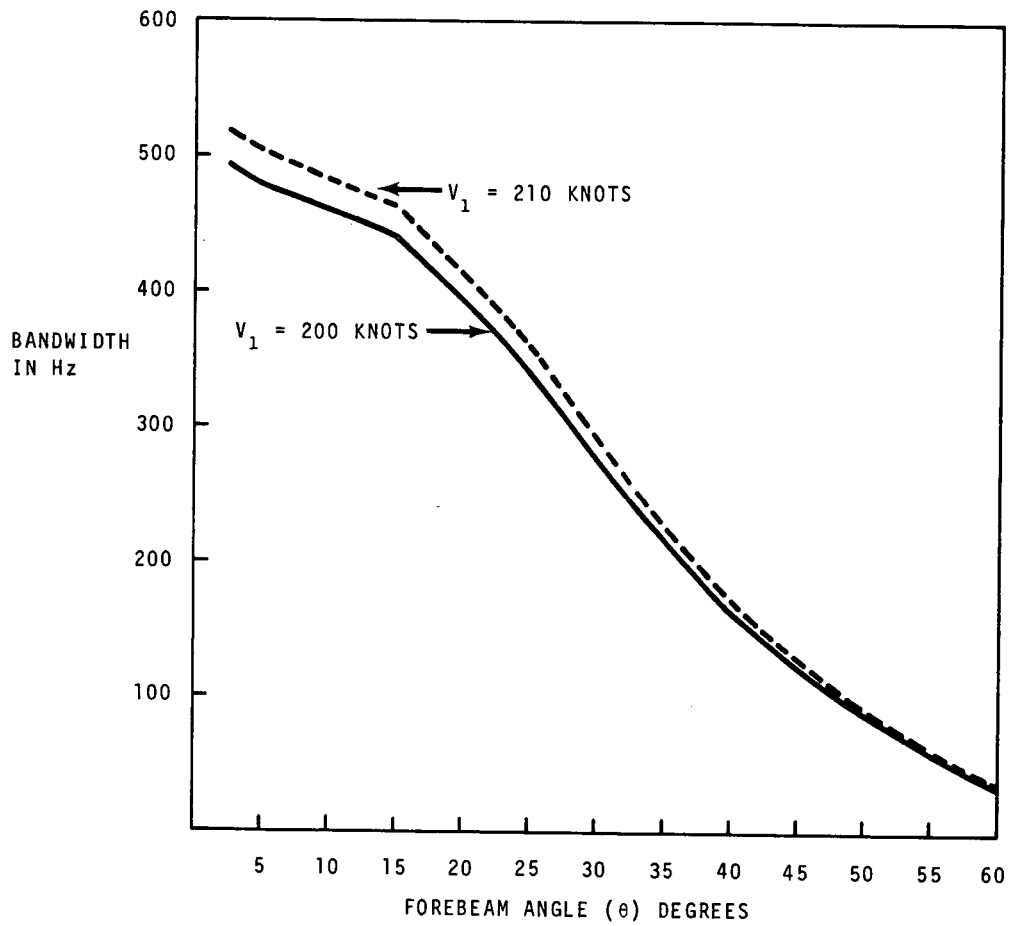


Figure 21. — Change in filter bandwidth due to change in aircraft velocity